Palaeogeography, Palaeoclimatology, Palaeoecology 637 (2024) 111986

Contents lists available at ScienceDirect

Palaeogeography, Palaeoclimatology, Palaeoecology

journal homepage: www.elsevier.com/locate/palaeo

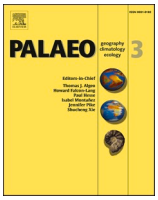

Controls on Quaternary geochemical and mineralogical variability in the Koora Basin and South Kenya Rift

R. Bernhart Owen [a,*], Nathan Rabideaux [b], Jordon Bright [c], Carolina Rosca [d,e], Robin W. Renaut [f], Richard Potts [g,h], Anna K. Behrensmeyer [i], Alan L. Deino [j], Andrew S. Cohen [k], Veronica Muiruri [h], René Dommain [g,l]

[a] Department of Geography and LEWI, Hong Kong Baptist University, Kowloon Tong, China
[b] Department of Chemistry, Rutgers University-Newark, Newark, NJ 07102, USA
[c] School of Earth and Sustainability, Northern Arizona University, Flagstaff, AZ 86011, USA
[d] Isotope Geochemistry Group, Department of Geosciences, Eberhard-Karls University of Tübingen, Germany
[e] Andalusian Institute of Earth Sciences (IACT), Spanish National Research Council (CSIC), Avenida de las Palmeras 4, 18100 Armilla, Granada, Spain
[f] Department of Geological Sciences, University of Saskatchewan, Saskatoon, SK S7N 5E2, Canada
[g] Human Origins Program, National Museum of Natural History, Smithsonian Institution, Washington, DC 20013, USA
[h] Department of Earth Sciences, National Museums of Kenya, Nairobi, Kenya
[i] Department of Paleobiology, National Museum of Natural History, Smithsonian Institution, Washington, DC 20013, USA
[j] Berkeley Geochronology Center, 2455 Ridge Road, Berkeley, CA 94709, USA
[k] Department of Geosciences, University of Arizona, Tucson, AZ 85721, USA
[l] Earth Observatory of Singapore, Nanyang Technological University, 50 Nanyang Avenue, 639798, Singapore, Republic of Singapore

ARTICLE INFO

Editor: Paul Hesse

Keywords:
Quaternary
Palaeolimnology
Geochemistry
Mineralogy
Volcano-tectonic controls
Climate

ABSTRACT

The South Kenya Rift is comprised of a series of N-S-oriented grabens with sediments that preserve an approximate one-million-year environmental history that reflects the interplay of climate, tectonism and volcanism. This study attempts to disentangle the relative roles of these major controls by comparing the geochemical records preserved in three sedimentary basins. The study focuses on the Koora Basin using bulk geochemical data in a 139-m-long core. This record is then compared with geochemical data and environmental histories from a 196-m-long core at Magadi and outcrops in the Olorgesailie Basin. Four climatic phases (1000–850; 850–470; 470–400; 400–0 ka) are recognised at Koora, which can also be distinguished in the Magadi and Olorgesailie Basins. However, inter-basin contrasts also suggest that additional, non-climatic factors influenced these geochemical histories, particularly during four intervals. These include 1) the Magadi Transition (MT; ~770–700 ka), 2) the Magadi Tectonic Event (MTE; ~540 ka), 3) the Koora Instability Period (KIP; ~325–180 ka), and 4) the Trona Precipitation Period (TPP; ~105–0 ka). Prior to the MT, Zr/TiO_2, La/Lu, Mo, As, V and Na/Ca in Magadi and Koora cores were similar but afterwards diverged. Major reductions in transition metals at Magadi during the MTE reflect tectonically-induced cross-rift drainage diversion. This contrasts with the Koora and Olorgesailie basins where these metals were constant from ~1000 to 300 ka. The KIP represents a significant increase in volcanic inputs to the Koora Basin and increased geochemical variability. Bromine (Br), which reflects peralkaline volcanic activity and/or evaporative concentration, is elevated during the KIP at Koora but is below detection limits in the rest of the Koora core. Br in the Magadi core does not correlate with that in the Koora record, suggesting contrasting accumulation processes. The TPP represents a phase of trona precipitation at Magadi but not at Koora. This difference partly reflects increased magmatic CO_2 rising along faults in the Magadi basin during a period of increasing aridity. Rare-earth element patterns indicate a major change at Magadi with many anomalies after about 325 ka to the present, caused by the development of hypersaline waters, which did not occur at Koora or Olorgesailie. The geochemical data from the three basins help to partially separate climatic controls from those related to volcanism, tectonism and local geomorphology.

* Corresponding author.
E-mail address: owen@associate.hkbu.edu.hk (R.B. Owen).

https://doi.org/10.1016/j.palaeo.2023.111986
Received 2 June 2023; Received in revised form 5 December 2023; Accepted 14 December 2023
Available online 21 December 2023

1. Introduction

Research into hominin origins and their cultural development has been stimulated by an exploration of links with climate change (Potts et al., 1999; Potts, 1998, 2013; Maslin et al., 2014; Potts and Faith, 2015; Potts et al., 2020). Consequently, papers on evolution have examined drivers of climate (glacial status, sea surface temperatures, Milankovitch cycles) using evidence from local basins and distant marine cores (Maslin and Trauth, 2009; Trauth et al., 2015). Cohen et al. (2009) pointed out the importance of detailed environmental datasets that can be related to palaeoanthropological sites on regional to local scales. However, these sites are often associated with fluvial sediments, palaeosols and erosional surfaces that do not typically preserve high-resolution, relatively continuous environmental histories over significant time intervals. Additional difficulties arise from analyses of sedimentary sections from different locations within a site, which reflects spatial variability as well as temporal change.

These problems have been recently addressed by coring lacustrine sequences close to palaeoanthropological sites. The Hominin Sites and Paleolakes Drilling Project (HSPDP) drilled five Plio-Pleistocene locations in Ethiopia and Kenya that lie close to important hominin sites (Cohen et al., 2016; Campisano et al., 2017), including cores from the South Kenya Rift at Magadi. Furthermore, the Olorgesailie Drilling Project (ODP) also recovered cores from the Koora Basin.

The Olorgesailie Basin (Figs. 1A, 2A) provides an outcrop record of hominin stone tools and palaeosols in fluvio-lacustrine sequences (Behrensmeyer et al., 2018). The Olorgesailie Formation (~1200–500 ka) contains Acheulean handaxes (Potts et al., 2018), a persistent form of stone technology that was replaced by Middle Stone Age artefacts in the overlying Oltulelei Formation (320–36 ka; Brooks et al., 2018). The environmental record for 500–320 ka is missing due to an erosional hiatus between the Olorgesailie and Oltulelei Formations, as well as several periods of erosion within the latter. Cores from the Koora Plain (ODP) and Lake Magadi (HSPDP) provide one-million-year records that include much of the 500–320 ka time interval.

The Koora Plain and Lake Magadi (Figs. 1A, 2B-C) lie ~20 km south and ~ 25 km southwest of Olorgesailie, respectively. Today, there are no lakes at Olorgesailie or Koora, with these rift sub-basins linked by the Ol Keju Nyiro River. A 139-m-long core (ODP-OLO12-1A [OLO12-1A]; Figs. 1A, 2D) from the Koora Plain includes a basal trachyte dated at 1084 ± 4 ka. Lacustrine sedimentation persisted until at least ~83 ± 3 ka (Deino et al., 2019). Lake Magadi lies in a separate basin to the west and dries seasonally to a trona pan. The Magadi core HSPDP-MAG14-2A (MAG-14-2A; Fig. 1A; Owen et al., 2018a) includes 194 m of lacustrine sediment (1078 ± 3.6–0 ka; Owen et al., 2019).

Prior core-based environmental records from the South Kenya Rift have been based on diatoms (Muiruri et al., 2021c), plant waxes and bulk organic matter (Lupien et al., 2021) from Koora, and for Magadi on diatom (Muiruri et al., 2021a), pollen (Muiruri et al., 2021b) and bulk geochemical evidence (Owen et al., 2019; Deocampo et al., 2021). This paper focuses on new geochemical and mineralogical studies from OLO12-1A (Fig. 1A), which are compared with previously published geochemical and mineralogical data from MAG14-2A (Owen et al., 2019) and Olorgesailie outcrops (Owen et al., 2011, 2014). Our major

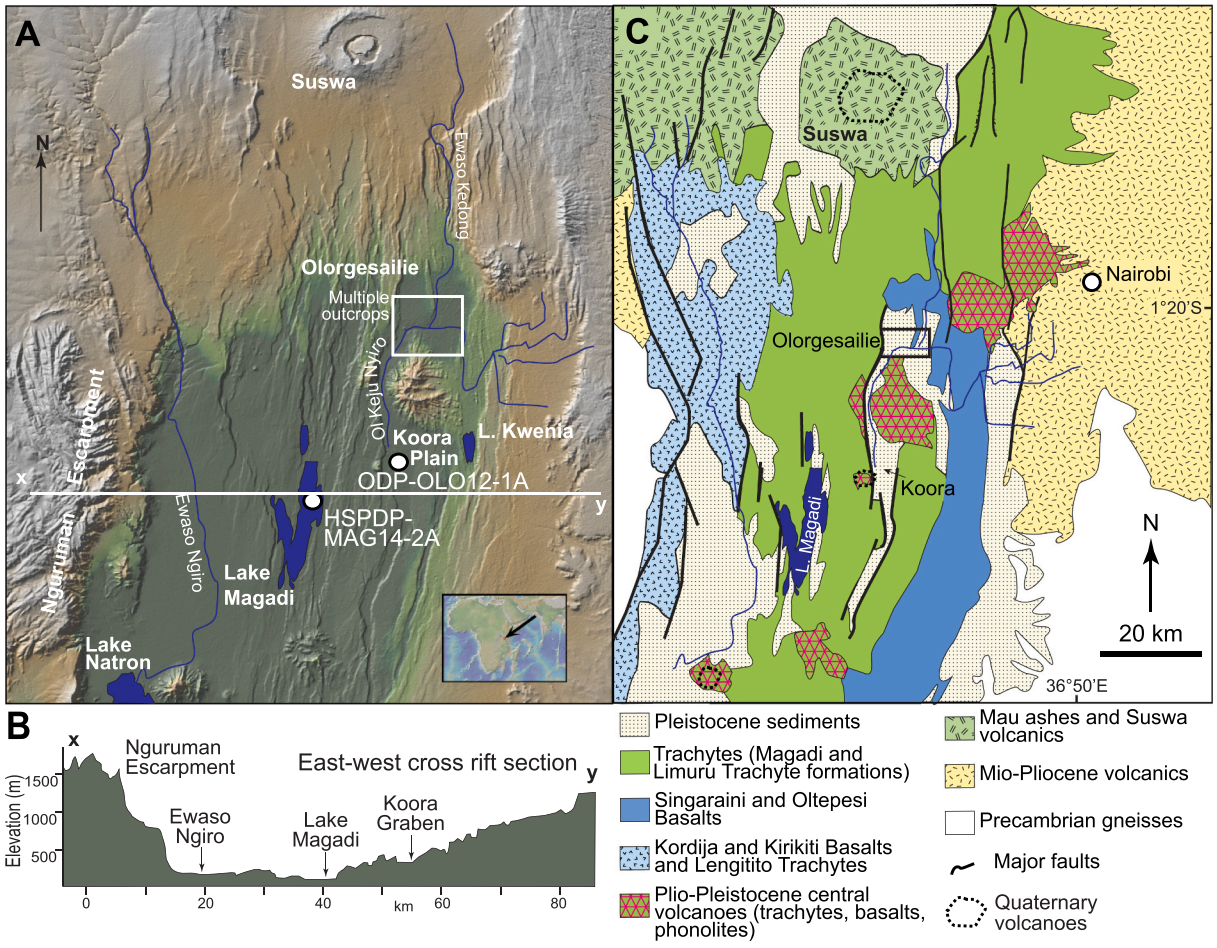

Fig. 1. Geography and geology of the southern Kenya Rift. A: Regional topography and core locations. Base map from GeoMapApp. B: Cross section showing the asymmetrical southern Kenya Rift. C: Simplified geology of the study region showing extensive outcrops of trachyte and basalt. Note basalts located at rift marginal areas. After Baker et al. (1977).

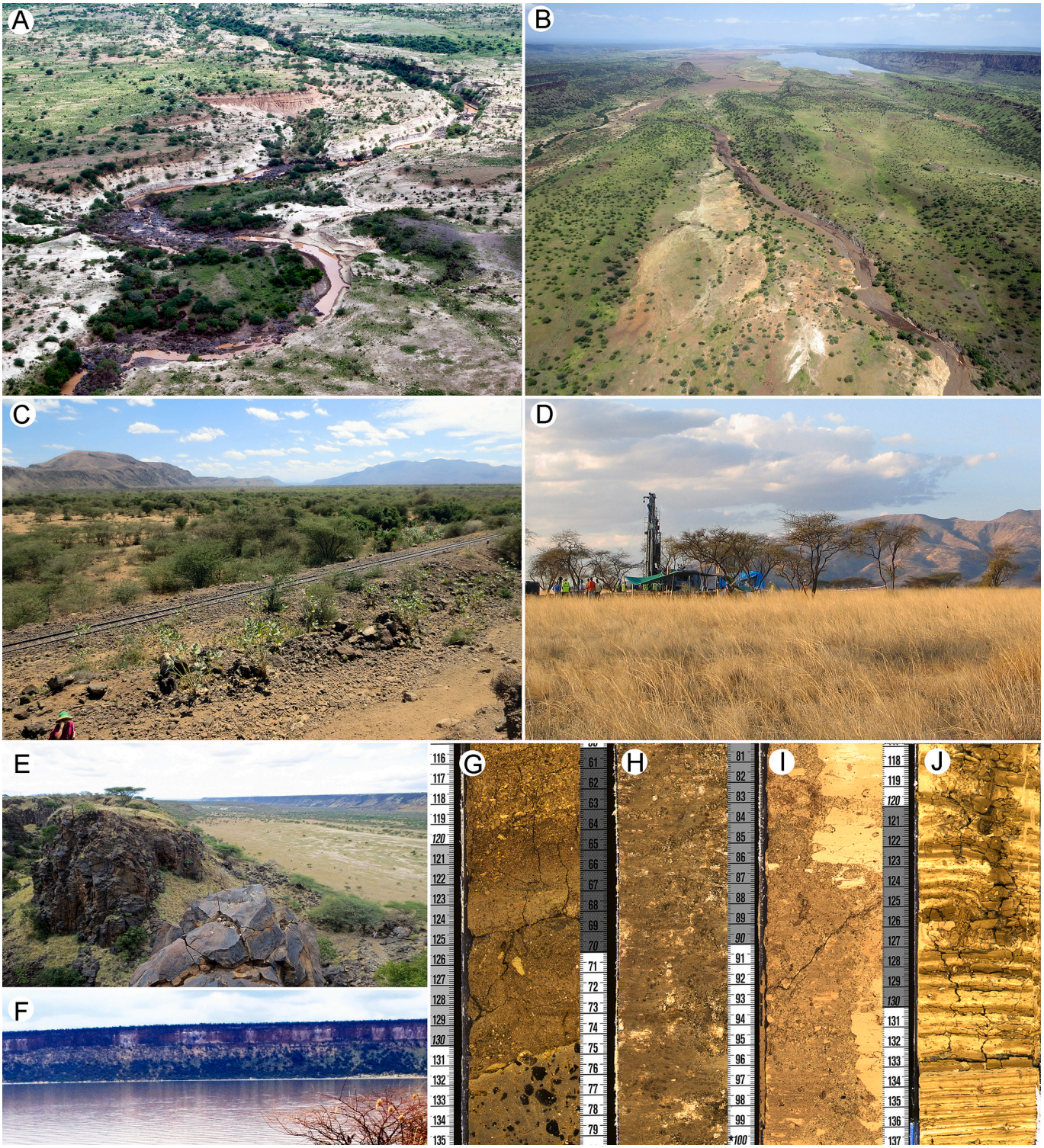

Fig. 2. The South Kenya Rift and Quaternary sediments. A: The Olorgesailie Basin with light coloured Olorgesailie Formation sediments. Note irregular fluvial erosion surface overlain by darker reddish-brown sediments of the Oltulelei Formation on the left (south) bank of the Ol Keju Nyiro River. Volcanic basement exposed left of river channel. B: View south over the South Kenya Rift with narrow north-south horsts and grabens hosting Nasikie Engida (top centre) and Lake Magadi (far distance). C: View north over the Koora Plain from the Magadi–Mombasa railway. The Pleistocene Oldoinyo Nyokie volcano to the west (left) is cut by a north-south-trending fault. Plio-Pleistocene Mt. Olorgesailie in the right background. D: OLO12-1A drill site. E: View north over the Siriati Graben (southern Koora palaeolake basin) with light patches of Holocene diatomaceous sediment. Note entrance to overflow channel to Magadi in left foreground. F: The flooded Kwenia Basin during a wet period (July 2018). In drier years the lake desiccates to a dry muddy playa. G–J: Selected OLO12-1A core segments. G: Section 82Q-2 (~152.6–152.4 mbs: metres below surface) – Silty pumice overlain by volcaniclastic sand and gravel. Inclined erosional break on the basal unit. H: Section 75Q-1 (~137.5–137.3 mbs) - diatomaceous clayey silt with carbonate nodules. I: Section 60Q-2 (~109.9–109.7 mbs) – massive subdiatomite cut by termite (?) burrow with clayey breccia infill. J: Section 63Q-1 (~117.7–117.5 mbs) - laminated to thinly bedded clay and diatomite. (For interpretation of the references to colour in this figure legend, the reader is referred to the web version of this article.)

aims here are to 1) explore the Koora geochemical record, 2) determine how changes in geochemical and mineralogical patterns through time do or do not correlate between all three basins, and 3) shed new light on the relative roles of climate, tectonism and volcanism in shaping past environments in the region.

2. Geological and geomorphological setting

The western South Kenya Rift is bordered by the ~2400-m-high Nguruman Escarpment and has its lowest point (~605 m) in the rift axis at Lake Magadi (Renaut and Owen, 2023). The eastern rift margin rises via a series of horsts and grabens (Fig. 1A,B) (Crossley and Knight, 1981). Near the western border fault, the post-Miocene sediment and volcanic fill ranges between 2000 and 3800 m (Masinde et al., 2023). The floor of the rift axis is dominated by Pleistocene flood lavas of the Limuru (2.01–1.88 Ma) and Magadi Trachyte (1.4–0.8 Ma) formations (Fig. 1C) (Baker et al., 1988) with the Kirikiti (3.1–2.5 Ma) and Kordiya (1.7 Ma) basalts outcropping at the Nguruman Escarpment (Crossley, 1979), and the Singaraini (2.33–2.31 Ma), Ol Keju Nyiro (1.79–1.64 Ma) and Oltepesi (1.65–1.4 Ma) basalts on the eastern side of the rift (Baker and Mitchell, 1976).

Eruption of Magadi Trachyte lavas infilled pre-existing grabens, resulting in a subdued volcanic palaeotopography upon which Quaternary sediments accumulated (Baker, 1958). Soon after their eruption they were fractured by north-south-trending faults. Today, grabens host: 1) the Olorgesailie and Oltulelei formations at Olorgesailie (Fig. 2A; Behrensmeyer et al., 2018; Potts et al., 2018); 2) the Oloronga, Green and High Magadi beds and Evaporite Series at Magadi (Fig. 2B; Owen et al., 2019); and 3) buried fluvial and lacustrine sediments at Koora (Fig. 2C,D; Potts et al., 2020; Muiruri et al., 2021c).

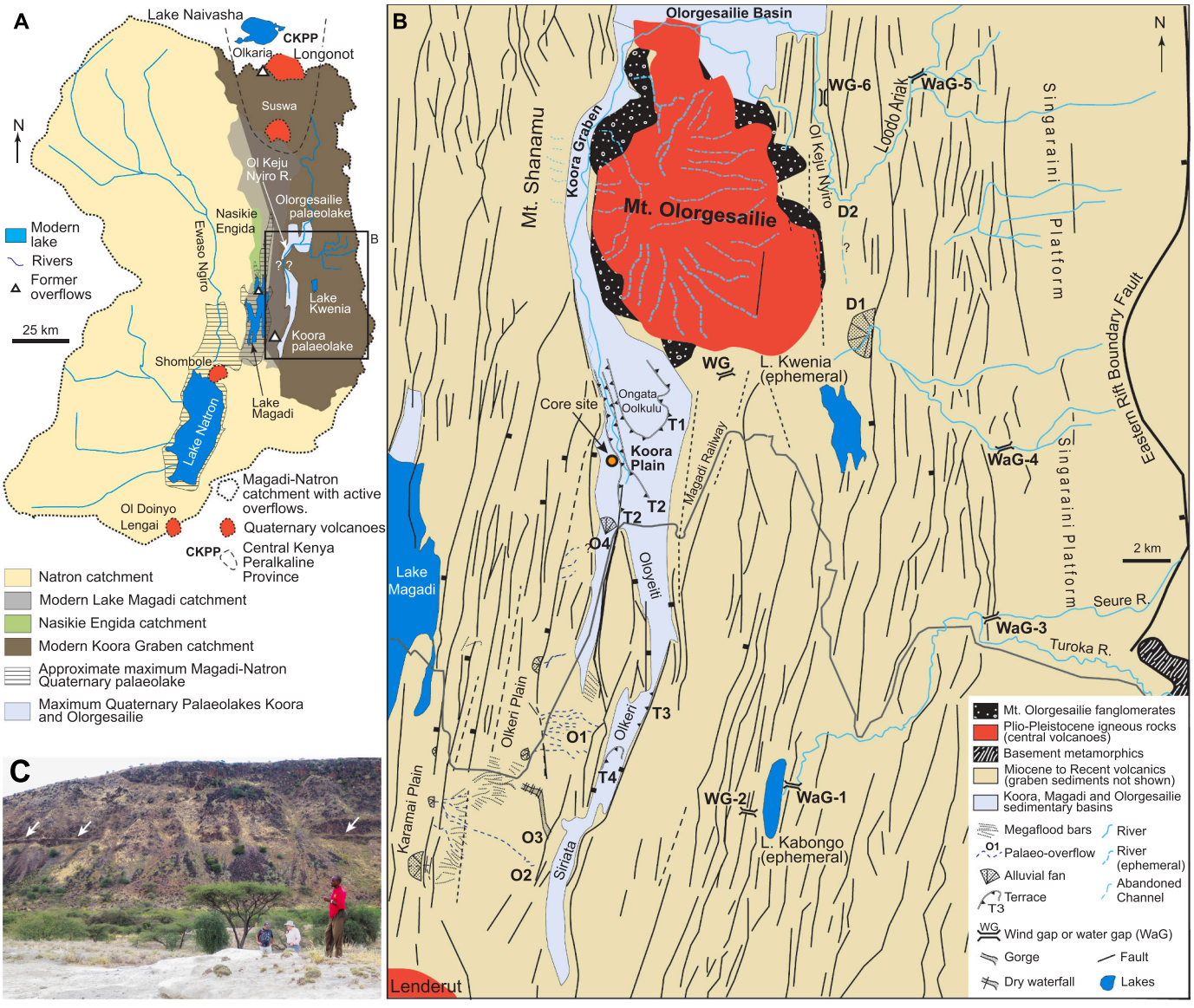

Fig. 3. Geomorphological setting. A: South Kenya Rift drainage basins. These were active in the African Humid Period and are of uncertain status at earlier times. The catchments combined to form a single large drainage basin (dotted line) intermittently during the Quaternary, with the Nasikie Engida Basin flowing east into an expanded northern Lake Magadi and the Koora palaeolake flowing into southeast Lake Magadi. Overflows marked. Lakes Magadi and Natron periodically formed a single large waterbody during the Middle to Late Pleistocene. B: Major landforms preserved east of the Magadi Basin. After Marsden (1979). Note four overflows (O1–O4) located at different elevations and therefore active at different times. The O3 outlet is shown in Fig. 2E. Megaflood bars are of uncertain age and formed by alternating, subparallel, cobble to boulder bars and aeolian silt on trachyte. Overflow channels and local drainage terminate at a series of fans on the Olkeri and Karamai Plains. Overflowa O1 and O2 may have been a sheetflow. D1 = alluvial fan and potential avulsion location. D2 = possible river capture of the Loodo Ariak river by the Ol Keju Nyiro river. C: Undated palaeoshoreline on eastern margin of the Koora Graben.

Table 1
Geochemical, mineralogical and biological parameters used in the Koora-Magadi-Olorgesailie basins and their interpretation. Note some parameters reflect multiple controls.

Indicator category	Elemental, mineralogical or biological tool	Main discriminations	References
Hydrological	Diatoms (SiO_2)	Salinity vs freshwater conditions	Muiruri et al. (2021a, 2021c)
	Biological calcite (ostracods)	Shallow water; moderately higher salinity	Cohen et al. (1983); Cohen (1986)
	Biological calcite $\delta^{18}O$ in (snail operculae)	Lower $\delta^{18}O$ values = calcification in fresher water - spring-fed lake margins/wetter periods	Talbot (1990); Hudson et al. (2017)
	$^{87}Sr/^{86}Sr$ (sediments and ostracods)	Single vs. multiple water sources; hydrological separation vs. interconnectivity	Ojiambo et al. (2003); Davies and Macdonald (1987); Bright (2017)
	Calcite and Mg-calcite	Moderately high water salinity	Halfman et al. (1989); Owen et al. (2019)
	Authigenic euhedral calcite	Precipitation in response to plankton blooms	Halfman et al. (1989); Ng'ang'a et al. (1998)
	Na_2O/CaO ratios	High vs. low water salinity	Owen et al. (2019)
	Zeolites (e.g., analcime, phillipsite)	High water salinity	Hardie and Eugster (1970); Herrick (1972); Eugster (1980)
	Elevated P_2O_5	Catchment weathering and concentration in plants/soils with erosion/ transport to lake	Owen et al. (2019); Ruttenberg (2014); Dericquebourg et al. (2015)
	Elevated Br	Biogenic activity; transport of plants to lakes; groundwater circulation	Neal et al. (2007); Chu et al. (2013); Allen et al. (1989); Owen et al. (2014)
	As, Bi	Hot springs, presence of Fe-oxides, sulphides	Varnavas and Cronan (1988)
	Increase in redox-sensitive elements (e.g., Mo, As, V)	Euxinic conditions (anoxic, saline and sulphide-rich)	Deocampo et al. (2021); Owen et al. (2018); Owen et al. (2019)
	Rare Earth Elements (REE)	Anomalies reflect hydrothermal springs and complexing with carbonate ions in soda lake	Johannesson and Lyons (1994); Owen et al. (2019)
Climatic	Pollen	Wetter vs. drier conditions; regional vegetation	Muiruri et al., 2021b
	Fluctuation in redox sensitive elements (e.g., Mo, As, V)	Euxinia cycles that coincide with high-orbital eccentricity	Owen et al. (2019)
	Br	Evaporative concentration in trona; Indian Ocean aerosols	Eugster (1980); Getenet et al. (2023)
	Diatoms	Indicators of pH, salinity and lake depth; correlation with global interglacials	Muiruri et al. (2021b).
Volcanic	Br (and other halogens), S	Increased volcanic activity, aerial transport; fluctuations reflect changing sources, wind directions or fluvial connections	Badertscher et al. (2014); Guevara et al. (2019)
	Tephra, glass shards	proximal or distal volcanic activity	Deino et al. (2019)
	As, Bi	Hydrothermal activity, hot springs	Ahoulé et al. (2015), Stauffer et al. (1980); Marchig et al. (1982)
	Analcime and phillipsite	Alteration products of tephra and zeolites in $Na\text{-}HCO_3$-rich waters	Rabideaux (2018); Owen et al. (2019)
Tectono-sedimentary	REE patterns and anomalies	Trachytic vs. basaltic components	Owen et al. (2019), Le Roex et al. (2001)
	Th, Ce, Sc, Zr	Trachyte or phonolite vs. basalt lithologies	This study; Le Roex et al. (2001)
	Mo/Sc vs. Th/Sc; Na_2O/Sc vs. Zn/Sc	(lithological mixing: mafic vs. more evolved components and oxic-anoxic excursions)	This study
	Zr/TiO_2, La/Lu	Changing source lithology due to tectonics; clastic input; tephra contributions	Deocampo et al. (2021)
	Increased transition metals (Co, Cr, Cu and Ni)	Mafic volcanics and transport to core site	This study; Owen et al. (2019)
	REE (e.g., Eu anomalies)	Contrasting sediment provenances	This study; Owen et al. (2019)

The Koora catchment (~5250 km^2) lies on the eastern side of the rift and includes the Olorgesailie Basin (Fig. 3A) at ~950–1025 m above sea level (masl). The Koora drill site lies at 845 masl, close to the termination of the Ol Keju Nyiro River (Fig. 3A). The Magadi Basin lies to the west in a tectonic sump at ~605 masl (Fig. 3B). Although separate catchments today, Baker (1958), Crossley (1976) and Marsden (1979) noted terraces (Fig. 3C), overflow channels, alluvial fans and dry waterfalls (Figs. 2E, 3B,C) that reflect past overflow from Koora to Magadi. Baker et al. (1988) and Muiruri et al. (2021c) also reported a catastrophic Late Pleistocene megaflood that crossed between the two basins. Roberts and Barker (1993) and Dommain et al. (2022) described aspects of the Early Holocene Olorgesailie-Koora-Magadi palaeodrainage, which they traced northward to Lake Naivasha. At times, Lakes Natron and Magadi were also linked (Hillaire-Marcel et al., 1986; Muiruri et al., 2021a). Today, neighbouring Lake Kwenia (Fig. 3A,B) periodically expands (Fig. 2F) and dries to a grassy plain. In contrast, saline Nasikie Engida has a small catchment (Fig. 3A) yet is a permanent lake (De Cort et al., 2019) maintained by hot spring inflow (Renaut et al., 2021).

3. Methods

Various geochemical, mineralogical and biological tools were used to assess environmental change (Table 1). The Koora bulk geochemical dataset (n = 268) was recovered from OLO12-1A (Fig. 1A). Drilling is described by Potts et al. (2020). The upper 27 m of friable silt were augured. Cores below that depth were shipped to the Continental Scientific Drilling (CSD) facility at the University of Minnesota, where they were cut into archive and working halves, logged, scanned and sampled. Lake Magadi geochemical samples (n = 344) were collected from core MAG14-2A, drilled in June 2014. Drilling operations were described by Cohen et al. (2016). An additional 239 samples were collected from outcrops in the Olorgesailie and Oltulelei formations (Olorgesailie Basin). Locations and sampling procedures are reported by Owen et al. (2014).

All major and trace elements were determined by Activation Laboratories Ltd., Ancaster, Ontario (Code 4E-exploration). Analytical techniques used for each element with detection limits are given in Electronic Supplementary Table S1. Loss on ignition (LOI) for $CaCO_3$, volatiles and organic matter content was determined at 1000 °C. Rare earth elements (REE) were normalised against C1 chondrites (Sun and McDonough, 1989).

Samples for X-ray diffraction (XRD) analyses were collected from OLO12-1A (n = 303) and MAG14-2A (n = 144) and carried out at Georgia State University using a PANalytical X'pert Pro MPD and Cu Kα-radiation (λ = 1.5418 Å) at 45 kV and 40 mA. Analysis measured 5–70° 2θ with 30-min scans. Diffraction patterns were determined using PANalytical High Score software with reference to the ICDD PDF-2

database, as well as Moore and Reynolds (1997) and Brindley and Brown (1980). Olorgesailie XRD analyses ($n = 33$) were conducted using a Bruker AXS D8 X-ray Diffractometer at Hong Kong Baptist University with Cu Kα-radiation and 20-min scans from 5 to 50° 2θ.

The W.M. Keck Isotope Laboratory (University of California at Santa Cruz) performed $^{87}Sr/^{86}Sr$ analyses on fish bone from five OLO12-1A horizons. Sediments were disaggregated in distilled water with repeated freeze-thaw cycles. Samples were digested in concentrated HNO_3. Strontium was separated using Sr resin with ^{87}Sr and ^{86}Sr measured by TIMS (Isotopx, UK) with single Re filaments and a Ta activator. Measurements are three-sequence dynamic mode. Isotope data were corrected for ^{87}Rb interference on ^{87}Sr, and internal mass bias to $^{87}Sr/^{86}Sr = 0.1194$. Repeated analysis of the standard solution NBS-987 yielded a $^{87}Sr/^{86}Sr$ ratio of 0.710247 ± 0.000006 (2σ).

Samples ($n = 10$) of snail operculae and ostracod valves from three OLO12-1A horizons were analysed for their $\delta^{18}O$ and $\delta^{13}C$ values at the University of Arizona's Environmental Isotope Laboratory using an automated KIEL-III carbonate preparation device coupled to a Finnigan MAT252 gas-ratio mass spectrometer. The samples were reacted with dehydrated phosphoric acid under vacuum at 70 °C. The isotope ratio was calibrated on repeated analyses of NBS-18 and NBS-19 standards. Stable isotope results are reported in standard delta (δ) notation where δ (‰) = $[(R_{sample}/R_{std})-1] \times 10^3$, and R = ratio of $^{18}O:^{16}O$ or $^{13}C:^{12}C$. R_{std} refers to the standard VPDB.

The OLO12-1A Bayesian age model was described by Deino et al. (2019) and is based on 22 $^{40}Ar/^{39}Ar$ dates from tephra and the basal Magadi Trachyte, supplemented by identification of the Brunhes-Matuyama (B-M) palaeomagnetic boundary. The model incorporates estimates for sedimentation and compaction for different lithologies and time associated with pedogenesis. MAG14-2A dating was described by Owen et al. (2018a) and includes two ^{14}C dates, nine $^{40}Ar/^{39}Ar$ tephra dates and an $^{40}Ar/^{39}Ar$ trachyte date. The MAG14-2A Bayesian age model also incorporates seven U-series chert dates and the B-M boundary. Olorgesailie samples from logged outcrops (Owen et al., 2008, 2014) were dated using $^{40}Ar/^{39}Ar$ techniques described by Deino and Potts (1990) and Deino et al. (2018).

4. Results

Fine-grained sediments dominate in all basins with the characteristics of 37 major facies summarised in Table 2. The different grabens display both similarities and contrasts in deposition. For example, freshwater lacustrine limestones (F1–F3; Table 2) are confined to older parts of the Magadi sequence, although calcareous deposits are present in all basins with tufa present at Olorgesailie. Highly diatomaceous facies (F5–F10) are common at Olorgesailie and in parts of the Koora core, but are absent at Magadi, except for moderately diatomaceous deposits ($<3 \times 10^6$ valves g^{-1}) in MAG14-2A. Zeolites are rare at Olorgesailie but common in the upper 105 m of the Koora core (F20–F24) and dominate in Magadi cores and outcrops (F25–31). Palaeosols (F11) are common at Olorgesailie and Koora but largely absent in the Magadi core. Chert and silicified mudstone (F31–F32) are common to abundant at Magadi but rare elsewhere. Opaline silica plant stems are common in Olorgesailie deposits (F12) younger than ~500 ka. Trona and nahcolite are confined to Lake Magadi and Nasikie Engida (F33–F37).

Fig. 4 shows PCA data for the three South Kenya Rift basins. Lithogenic elements and biogenic silica (mainly diatoms) are generally represented by positive axis 1 values in all basins reflecting clastic inputs from the surrounding trachytic and basaltic rocks and lacustrine settings. Negative axis 1 values represent elements associated with carbonate sediments (trona, nahcolite, lime mud, limestone), which differ between the basins. At Koora, the alkali earth metals CaO, MgO, Sr, Be and Ba and the metal Cs, as well as Loss on Ignition (LOI), show negative values with the two majors and LOI reflecting calcite, high-Mg calcite and minor dolomite.

Several clusters of elements can be distinguished at Koora. The metals V, Sc, Cr and TiO_2 plus Ba plot with moderately negative axis 1 and positive axis 2 values, close to P_2O_5. In contrast, Ni, Co, Sb, Cu, Cd, Pb and Bi display strongly positive axis 2 and strongly negative axis 3 values. Biological silica, Al_2O_3, Fe_2O_3 and the lanthanides La, Y, Nd, Eu, Ce, Sm, Yb and Lu, together with Zr, Hf and Th, show strongly positive axis 1 values, slightly negative to positive axes 2 values and moderately positive axis 3 plots. Both metals and non-metals (Na_2O, K_2O, MnO, Mo, Tb, Ta, S) plot with positive axis 1 and negative axis 2 and 3 values with U, Br, As and Au plotting close to zero on axis 1 and negatively on axes 2 and 3. These relatively tight clusters are not clearly distinguishable in the Olorgesailie or Magadi Basins. However, the Olorgesailie deposits show a similar separation between CaO/LOI (calcite, high-Mg calcite), lithogenic elements and biogenic silica. In contrast, the Magadi basin displays significant differences, notably with strongly negative Na_2O on axis 1 and positive CaO (axes 1 and 2), reflecting the abundance of trona in this basin.

Koora bulk geochemical data (Table S1), a lithological log, mineralogy, magnetic susceptibility, and major and trace element data are plotted against OLO12-1A core depth in Fig. 5. The Bayesian chronology indicates relatively slow sedimentation rates in the lower core through to ~410 ka, followed by somewhat faster deposition at ~410–240 ka and more rapid though variable rates in younger sediments. Detrital albite and K-feldspar are common throughout, with anorthoclase in mineral zones MZ2 to MZ5.

MZ1 (162–147 m; ~1010.5–682.3 ka) and MZ2 (147–112.5 m; ~682.3–289.2 ka) contain abundant feldspar, common silica polymorphs (quartz, tridymite, cristobalite) and intermittent smectite with MZ2 distinguished by sporadic calcite, Mg-calcite and dolomite, with anorthite absent. Silica and carbonate are lacking in MZ3 (112.5–101 m; ~289.2–246.8 ka), which includes the first appearance of analcime. MZ4 (101–98.5 m; 246.8–237.2 ka) contains common carbonates with analcime absent. MZ5 (98.5–45.5 m; ~237.2–184.0 ka) is distinguished by abundant zeolites (mainly analcime and phillipsite) with minor carbonates, smectite and silica. MZ6 (45.5–38 m; ~184.0–109.3 ka) lacks zeolites with analcime in a few samples in MZ7 (38–27 m; 109.3–83.5 ka). Quartz and tridymite are common in MZ6 and MZ7, with smectites absent and carbonates intermittently present. Low magnetic susceptibility (MS) values reflect diatomaceous sediments and diatomites (e.g., 117 m in MZ2).

Calcium carbonate is reflected in increased CaO and LOI, with MgO also increasing in many, but not all, carbonate-rich deposits. SiO_2, Al_2O_3, Fe_2O_3, Na_2O and K_2O decline in carbonate-rich horizons. TiO_2 and P_2O_5 are comparatively abundant but variable in MZ1 and MZ2, with smaller increases in MZ6 and MZ7. MnO shows little variation except for higher values in a few carbonate-rich horizons.

The zeolite-rich MZ3 and MZ5 display low Ba, Be, Co, Cr, Cs, Cu, Ni, Sc, Sr and V concentrations, all of which are more enriched in MZ1, MZ2 and MZ6. Mo and S reach peak enrichments in MZ3, MZ5 and MZ7 but are scarce or below detection in MZ1, MZ2 and MZ6. MZ4 contains low concentrations of Ag, Hf, Mo, Th and REE elements. Au and W are generally below detection limits, except at 106 m and 33.5–36 m, respectively. Se concentrations are below detection, except in MZ2 and MZ5. Bi and Br show little correlation with the mineral zones. Bi is present in higher concentrations at 50.25–72.5 m. Br is abundant between 89 and 122.5 m. Bi, Cd, Co, Cu, Ni, and Pb show very high values in tuffs between 52 and 55 m. Other elements exhibit similar concentrations throughout.

Six strontium isotope fish bone analyses (54.8–129.24 m) varied within a narrow range ($^{87}Sr/^{86}Sr = 0.705120–0.705502$; Table 3). $\delta^{18}O$ values from ten biological calcite samples (99.85–111.43 m) were 1.04–3.00‰ for ostracods and − 2.04–1.12‰ for operculae. Ostracod $\delta^{13}C$ were − 1.19–3.45‰ with operculae values of −0.66–0.71‰.

Table 2
Major sedimentary facies in the South Kenya Rift. Diatomaceous sediment terminology after Owen (2002).

Primary lithology	Lithology, structure and diatom content	Environment	Olorgesailie	Koora core	Magadi core	Magadi Basin	Nasikie Engida core
F1. Gastropod limestone.	Limestone with abundant in situ and reworked gastropods shells in micritic and sparitic matrix. Shallow-water diatoms, ostracods.	Shallow to moderately deep, fresh lake.			✓	✓	
F2. Carbonate grainstone.	Bedded fine to coarse carbonate sand grainstone (shells, trachyte). Weakly laminated in a few horizons.	Shallow to moderately deep, fresh lake.			✓		
F3. Carbonate mud.	Poorly bedded, light brown carbonate mud. Pyrite grains (1–1.5 cm) with bluish rims. Light coloured grains of chert. Chert with open vugs.	Moderately deep or deep, fresh to mildly saline lake.			✓		
F4. Tufa.	Bedded and stromatolitic tufa. Sparry calcite and micrite. Tufa encrusted reeds, leaves and twigs. Diatomaceous.	Springs, rivers and shallow ponds.	✓				
F5. Massive subdiatomite.	Homogeneous to vaguely bedded, white to pale yellow. Diatoms abundant, clay or silt, bioturbated.	Shallow to deep lakes with low clastic inputs.	✓	✓			
F6. Massive calcareous subdiatomite/diatom silt.	Homogeneous to bedded, diatoms present, bioturbated. Carbonate variable, generally from 10 to 90%.	Saline or moderately saline lake.	✓	✓			
F7. Bedded Clayey/silty subdiatomite.	Alternating diatomite with clayey or silty diatomite. Locally interbedded with pumice; may be calcareous.	Moderately deep to deep freshwater lake.	✓				
F8. Laminated clay and diatomite.	Similar to F7, but with mm-scale diatomite and clayey diatomite laminae.	Deep freshwater lake.	✓				
F9. Diatomaceous silt/ clayey silt/sandy silt.	Massive to weakly bedded/laminated silt, clayey silt, sandy silt. Diatoms up to 70% by volume. Siliciclastics and volcanic glass.	Fresh to moderately saline lakes and wetlands.	✓	✓			
F10. Reworked diatomite, subdiatomite.	Massive or irregular bedding. Diatoms commonly broken; intraclasts and/or rhizoliths may be present.	Lake marginal, emergent lake sediments.	✓				
F11. Pedogenic silt/ clayey silt.	Diatomaceous/non-diatomaceous silt/clay. Carbonate nodules, peds, horizontal and vertical cracks, rhizoliths. Volcanic glass, siliciclastics.	Pedogenically altered lake and floodplain deposits.	✓	✓			
F12. Cherty-opaline rhizoliths in diatom silt.	Homogeneous silt with variable diatom content (sometimes zero). Cherty and opaline plant stems, burrows.	Shallow wetlands, subject to desiccation.	✓				
F13. Brecciated clay/silt (diatomaceous).	Brecciated massive to laminated sediments. Variable sediment composition, carbonates may be present.	Reworked lacustrine or floodplain sediments.	✓	✓			
F14. Silty/sandy pumice.	Matrix- to clast-supported pumice and siliciclastics. Poor to moderate sorting, common rounded pumice (generally <3 cm).	Airfall ash/pumice into lake or fluvial transported to lake.	✓	✓			
F15. Silty sand and sandy silt.	Poorly sorted, weakly laminated/bedded, massive siliciclastic silt and fine sand. Clay, pumice, volcanic glass present	Shallow lake, possible periods of exposure.	✓	✓	✓	✓	
F16. Friable, clayey, silty and gravelly sand.	Moderately to poorly sorted volcaniclastic clay, silt, sand and gravel. Loose and massive.	Floodplain deposits, aeolian contributions?	✓	✓	✓	✓	
F17. Ash.	Well-sorted, laminated ash; laterally extensive. May have burrows, rhizoliths.	Airfall ash.	✓	✓	✓	✓	
F18. Boxwork evaporite silt.	Evaporite pseudomorphs, crack fills, fluid-escape structures.	Playa or evaporative mudflat.	✓			✓	
F19. Volcaniclastic silt/ sand/gravel.	Clast-supported pumice and sandy silt. Common volcanic glass, calcareous with clay, root traces, burrows, cut-and-fill structures.	Shallow water to subaerial. Fluvial influence.	✓	✓	✓	✓	
F20. Zeolitic silty sand.	Analcimic silty sand. Clay laminae. Volcanic glass abundant with siliciclastics. Granule-size pumice.	Shallow (?) saline lake.		✓			
F21. Zeolitic silty clay and clayey silt.	Analcimic silty clay, finely bedded, paired clay laminae. Scattered pumice. Volcanic glass, siliciclastics, varied zeolites, pyrite.	Saline lake.		✓	✓		
F22. Massive zeolitic clay.	Massive to weakly bedded light green zeolitic clay. Wispy banding. Scattered and subhorizontal laminae of white crystals and pyrite.	Saline lake.			✓		
F23. Zeolitic laminated silt.	Zeolitic laminated silt, horizontal/ripple laminae. Glass/siliciclastics.	Saline lake.		✓			
F24. Zeolitic gravelly sand.	Massive analcimic silty and gravelly sand. Glass, pumice and siliciclastics. Carbonate clasts.	Debris flow into saline lake.		✓	✓		
F25. Massive silty ash.	Massive dark grey zeolitic silt. Subhorizontal fractures allude to layering. Local chert nodules. Pyrite at some levels.	Saline lake.		✓	✓		
F26. Black clay.	Massive to weakly laminated clay. Diffuse organics; rare plants, fine clastics. White (calcite?) crystals, zeolites, pyrite, chert.	Fresh to moderately saline lake.			✓		

(*continued on next page*)

Table 2 (*continued*)

Primary lithology	Lithology, structure and diatom content	Environment	Olorgesailie	Koora core	Magadi core	Magadi Basin	Nasikie Engida core
F27. Laminated silt and clay.	Green-grey, non-diatomaceous laminated silt/clay; zeolitic or calcitic. Convolute laminae, microfractures. Pollen, pyrite, patchy chert.	Deep, fresh to moderately saline lake.			✓		
F28. Bedded gravel.	Coarse siliciclastics. Massive to well bedded. Pyrite or glass. Zeolitic fining-up sequences; inclined bedding, erosional scours.	Fluvial (with reworked lake sediments).		✓		✓	
F29. Matrix-supported volcaniclastics.	Matrix-supported rounded pumice. Matrix includes volcanic glass, clay, siliciclastics, zeolites, pyrite, root channels.	Debris flow into fluvial and alluvial fan settings.		✓	✓		
F30. Alternating clay and magadiite.	Laminated zeolitic clay and magadiite in upward-fining cycles. Burrowed magadiite. Magadiite converts to chert.	Seasonally flooded playa/ shallow saline lake.			✓	✓	
F31. Silicified mudstone.	Silicified bedded zeolitic mud. Pyrite present at some levels.	High-silica saline lake.			✓		
F32. Chert.	Bedded, lensoid to nodular cherts. Compaction around chert indicates early lithification. Serrated or reticulate surface textures.	High-silica saline lake. Chert replaces magadiite, trona, gel.			✓	✓	
F33. Massive mud with trona.	Black zeolitic mud with mm-scale trona crystals. Interbedded with massive or bedded trona. Some larger trona crystals.	Saline alkaline lake.			✓	✓	
F34. Bedded trona.	Bedded trona (1–3 cm layers) with clusters of radiating crystals. (Sub)horizontal dissolution surfaces.	Very shallow (< 1 m?), hypersaline, alkaline lake.			✓	✓	
F35. Massive trona.	Massive recrystallized trona. Crystals <1 to 3 cm with mostly random orientations. Interstitial greenish zeolitic black mud is common.	Hypersaline lake.			✓	✓	
F36. Alternating nahcolite and silt.	Bedded alternations of nahcolite and diatomaceous, erionitic silty mud with nahcolite crystals.	Spring-fed shallow saline lake with high silica.					✓
F37. Laminated erionitic mud.	Laminated diatomaceous and feldspathic erionitic silty mud.	Permanent spring-fed saline lake with high silica.					✓

5. Discussion

5.1. Geochemical stratigraphy, OLO12-1A, Koora Basin

5.1.1. Sediment sources and mixing

Lithological sources in the Koora catchment include the Magadi Trachyte, Singaraini Basalt and Oltepesi Basalt formations (Fig. 1C). The proximity of deeply eroded Plio-Pleistocene Mt. Olorgesailie suggests it was also a contributor of alkali basalt, mugearite, benmorite, trachyte, trachyphonolite and nephelinite (Baker, 1987). Distal lithologies include Mio-Pliocene volcanics from the rift shoulder and Mau ashes and peralkaline volcanics in the Naivasha area to the north. $^{40}Ar/^{39}Ar$ single-crystal ages of xenocrystic feldspars in OLO12-1A (Fig. 11 in Deino et al. 2019) range up to ~8 Ma, and support derivation of a variety of materials from areas proximal to Olorgesailie and Koora, as well as distal areas.

Figure 6A plots Th, Ce and Sc against Zr and shows a clear distinction between trachyte and basalt (Le Roex et al., 2001). Core sediments plot between trachyte and basalt compositions, although with slightly higher Th. Comparison of data from MZ2 and MZ6–7 indicate that the former is associated with lower Zr concentrations whereas MZ6–7 is characterised by higher values, closer to trachyte.

Sample discrimination is best for Sc with low core sediment values resembling trachyte and phonolite (< 5 ppm) rather than basalt (> 30 ppm). Individual mineral zones can be separated in the Sc plot with MZ1 and MZ2 containing higher Sc concentrations than MZ5 and the lowest values associated with MZ3 and MZ4. Overall, the data indicate mixed basalt-trachyte contributions with Sc suggesting dominance by trachytes and/or phonolites.

Binary plots of Sc-normalised trace elements (Fig. 6B) suggest possible *syn*- or post-depositional geochemical processes. For example, redox sensitive molybdenum is reported from Lake Magadi cores (Deocampo et al., 2021) with plots of Mo/Sc against Th/Sc, Na_2O/Sc and Zn/Sc at Koora clearly defining two trends. Rift volcanics data for Mo is scarce (Fig. 6B) but one trend likely reflects lithological mixing between mafic and more evolved volcanic components with contrasting Sc contents. The other probably represents a process-related excursion (e.g., anoxic-oxic effects, metal capture and extraction, contrasts between saline and freshwater settings).

5.1.2. Geochemical zones – Environmental implications

Scandium depth profiles resemble those of TiO_2 and Al_2O_3, reflecting detrital controls. Fig. 7 normalises elements using Al_2O_3 and plots the results against age. It also compares these data with the mineralogical zones (MZ1–MZ7), diatom-inferred environments (Muiruri et al., 2021a, 2021b, 2021c) and the palaeosol record (Potts et al., 2020). Nine geochemical zones (GZ1–GZ9) were visually distinguished using variations in SiO_2, Na_2O and CaO. High positive r-values between Al_2O_3 and Fe_2O_3 (0.79), K_2O (0.68), Na_2O (0.56) and TiO_2 (0.43) represent fluvial and aeolian lithogenic inputs (Owen et al., 2019). Lower positive correlations for SiO_2 (0.28) reflect the combined influence of lithogenic and biological (diatoms, sponge spicules) contributions. Al_2O_3 shows a strong negative correlation with CaO (−0.70), MgO (−0.50) and LOI (−0.78). Euhedral carbonate in parts of the core implies that some precipitation took place in a water column.

GZ1 to GZ2 broadly coincide with MZ1, which is characterised by abundant feldspars and an absence of authigenic minerals (Figs. 5, 7). Diatomaceous silt with low MS values (Fig. 5) dominates in GZ1 (~1010–890 ka), which is also associated with lithogenic elements and higher silica than GZ2. Low Na_2O and CaO suggest fresh water (Owen et al., 2019), which is supported by the presence of shallow-water diatoms that indicate low conductivity and pH 7.5–8.5 (Muiruri et al., 2021c).

Major and trace elements are more variable in GZ2 (~890–710 ka), which is defined by lower SiO_2 and minor quartz and tridymite in sandy facies. Muiruri et al. (2021c) reported low diatom abundance with a diatom-based correspondence analysis (CA) (Fig. 7) indicating greater water depths. Both CaO and Na_2O increase slightly but remain low

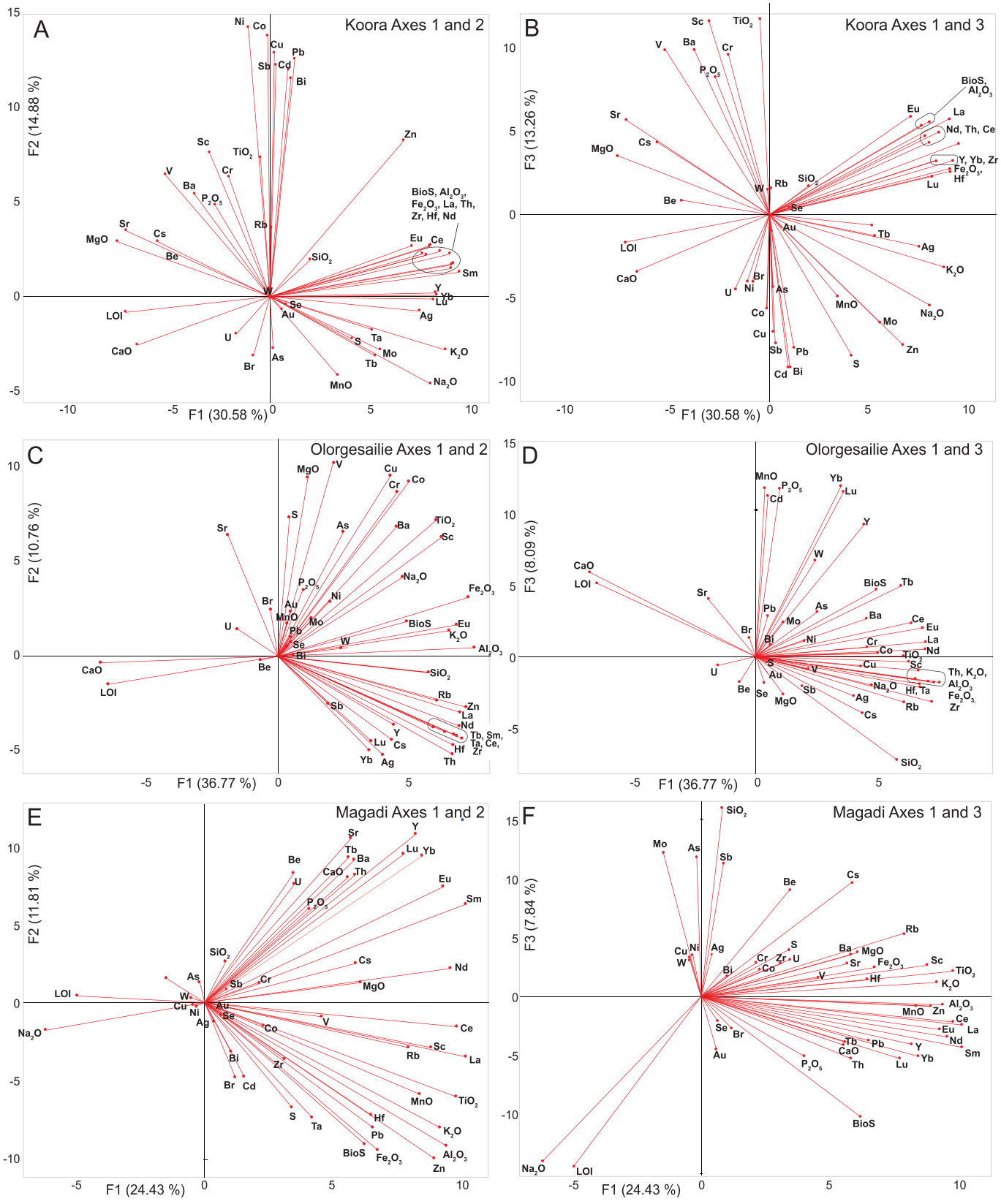

Fig. 4. PCA diagrams of elemental data for the Koora, Olorgesailie and Magadi basins. Axis 1 separates lithogenic elements with positive scores from carbonates with negative scores. Note that the Koora carbonates are characteristically CaO- and MgO-rich (calcite, Mg-calcite, dolomite), with Olorgesailie dominated by CaO (calcite). In contrast, the negative part of the Magadi axis 1 is dominated by Na_2O, reflecting abundant trona.

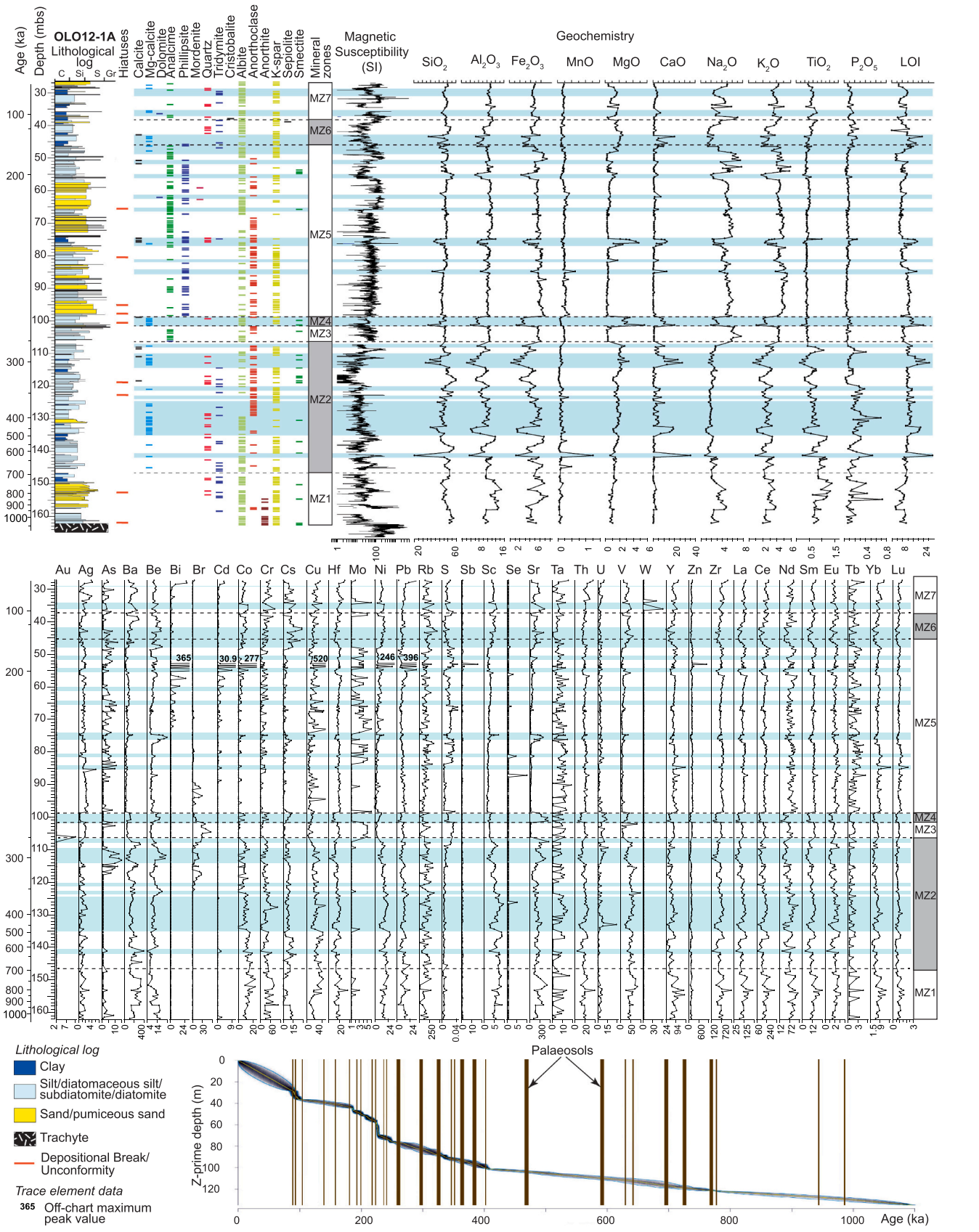

Fig. 5. Sedimentological, mineralogical and geochemical stratigraphy of OLO12-1A. This is a depth plot. Core chronology is shown to bottom right using '*Z*-prime data', which incorporates differing sedimentation rates and compression effects (Deino et al., 2019). Note varying sedimentation rates with rapid accumulation at about 250–200 ka; palaeosols (hiatuses) are also shown (Potts et al., 2020). Blue bands highlight increased CaO. (For interpretation of the references to colour in this figure legend, the reader is referred to the web version of this article.)

Table 3
Core ODP-OLO12-1A isotope data.

$^{87}Sr/^{86}Sr$ ratios in fish bones					
Raw depth (MBS)	Sample Identification	Mean	stdev (1σ)	n*	Ostracods present?
54.80	OLO12-1A-39Q-1 101.5–104.5 cm	0.705502	0.000020	118	no
54.80	OLO12-1A-39Q-1 101.5–104.5 cm (d)	0.705490	0.000023	116	no
99.89	OLO12-1A-56Q-2 38.5 44.5 cm	0.705130	0.000027	114	yes
111.42	O12-1A-61Q-2 105 111 cm	0.705292	0.000016	120	yes
122.94	OLO12-1A-65Q-1 4753 cm	0.705499	0.000017	120	yes
129.24	OLO12-1A-70Q-2 41.4–47.5 cm	0.705120	0.000017	121	no

$\delta^{18}O$ and $\delta^{13}C$ values from biologic calcite				
raw depth (MBS)	Sample Identification	Material	$_{\delta}18_{O}$ (‰, VPDB)	$_{\delta}13_{C}$ (‰, VPDB)
99.87	OLO12-1A-56Q-2 38.5–41.5 cm	*Lim. africana*	3.00	0.16
99.87	OLO12-1A-56Q-2 38.5–41.5 cm	*Lim. africana*	2.35	−0.29
99.87	OLO12-1A-56Q-2 38.5–41.5 cm	*Lim. africana*	2.07	−0.07
99.87	OLO12-1A-56Q-2 38.5–41.5 cm	*Cypridopsis* sp.	1.65	2.99
99.89	OLO12-1A-56Q-2 38.5–44.5 cm	opercula	−1.12	−0.66
99.89	OLO12-1A-56Q-2 38.5–44.5 cm	opercula	−2.04	0.71
99.90	OLO12-1A-56Q-2 41.5–44.5 cm	*Lim. africana*	1.89	−0.49
99.90	OLO12-1A-56Q-2 41.5–44.5 cm	*Cypridopsis* sp.	2.84	3.45
111.42	OLO12-1A-61Q-2 108–111 cm	*Lim. africana*	1.50	−1.02
111.42	OLO12-1A-61Q-2 108–111 cm	*Lim. africana*	1.04	−1.19

*Sample solutions were read 128 times. Any $^{87}Sr/^{86}Sr$ ratios that fell outside 2σ of the original mean were removed and the remaining readings were averaged again. This process was only performed once.

overall, suggesting continued low salinity. Lithogenic elements are more variable than in GZ1, perhaps due to grain-size effects given the course siliciclastics.

GZ3 (~710–595 ka), GZ4 (~595–560 ka), GZ5 (~560–455 ka) and GZ6 (~455–400 ka) correlate with lower to middle MZ2 and are characterised by intermittent CaO peaks that mostly correlate with Mg-calcite (Figs. 5 and 7), elevated P_2O_5 and increased saline diatom taxa. Authigenic Mg-calcite may have precipitated in response to phytoplankton blooms favoured by moderate increases in salinity and/or nutrient inputs during regressions. Today, micritic lacustrine carbonates are precipitating in moderately saline Lake Turkana (Halfman et al., 1989), triggered by photosynthetic microbial blooms (Ng'ang'a et al., 1998). Owen et al. (2019) also reported variable P_2O_5 in Magadi cores, suggesting release following weathering, uptake by plants and concentration in soils (Ruttenberg, 2014) with subsequent erosion and transport delivering phosphate to the palaeolake (cf. Dericquebourg et al., 2015). The percentage of CaO is high in GZ4 and GZ6, which correlate with major diatom-inferred regressions (Fig. 7).

GZ7 (400–184 ka) correlates with upper MZ2 to MZ5 and displays variable CaO concentrations. Mg-calcite and calcite dominate in MZ2 and MZ4, giving way to analcime (MZ3), and then analcime and phillipsite (MZ5). The presence of zeolites suggests a transition towards higher pH. The inverse correlation between analcime and $CaCO_3$ (inferred from Ca and LOI) suggests that during deposition the salinity and (or) alkalinity of the water had exceeded the alkalinity pathway branchpoint (chemical divide) and there was little to no free Ca available (Hardie and Eugster, 1970). Subzone GZ7a is relatively stable except for CaO, which suggests fluctuating fresh to moderately saline water, an inference supported by diatom conductivity data (Fig. 7). GZ7b contains higher and variable SiO_2 concentrations, a major increase in Br (up to 55 ppm), decreasing and variable TiO_2 and P_2O_5, and increasingly abundant and fluctuating Na_2O with peaks (~260, 290 and 320 ka) that correlate with diatom-inferred salinity increases. Bromine has been attributed to volcanogenic, biogenic and oceanic aerosol transport (Table 1). However, these latter mechanisms are unlikely to explain the two-orders-of-magnitude increase at Koora or the very low Br concentrations through the rest of the core. A volcanic source might explain the Br content given that Deino et al. (2019) reported increased tephra and sedimentation rates in GZ7b and GZ7c (see Section 5.2).

Both As and Bi fluctuate significantly in GZ7b and GZ7c with the latter being the most varied interval in the core. Arsenic in African waters has been attributed to the presence of iron oxides, sulfides (pyrite, arsenopyrite, chalcopyrite), volcanic rocks, geothermal water (Ahoulé et al., 2015) and groundwater with pH > 8 (Rango et al., 2013). It has also been cited as an indicator of hydrothermal activity in oceanic and continental studies (Stauffer et al., 1980; Marchig et al., 1982). Steffánsson and Anórsson (2005) reported increased As in hot springs as temperatures increased with a tenfold rise in areas with acidic rocks rather than basalt. Global studies of Bi indicate lower concentrations than As with means of 31 ppb in crustal tholeiitic basalts, ~66 ppb in alkali rocks, and 600 ppb in pneumatolytically altered granites, although it may constitute a few ppm in apatite or sphene (Heinrichs et al., 1980). Mean concentrations in sedimentary rocks are also low (80–110 ppb). At Koora, Bi concentrations distinguish GZ7c from all other zones, except GZ9. Bismuth is also below detection (< 2 ppm) in almost all Olorgesailie and Magadi sediments (Owen et al., 2011, 2018b), suggesting that elevated Bi formed in localised settings, perhaps hot springs(?). Varnavas and Cronan (1988) observed that sediments near Aegean submarine hydrothermal springs contained moderately elevated Bi (108 ppb) close to vents and that As concentrations increased (up to 927 ppm) a few tens of metres away from springs, reflecting scavenging by Fe-oxides and the prevailing pH, Eh and temperature.

Increased tephra in GZ7c correlates with MZ5 and increased phillipsite with analcime also common. At Magadi, Surdam and Eugster (1976) reported that analcime forms as an alteration product of tephra or other zeolites in the presence of Na-HCO_3-rich waters with a high Na and low SiO_2 activity, and noted that phillipsite develops in fluvial and lake marginal settings where it is associated with alkaline groundwater when Ca is available, lower silica activity and higher Na/K ratios (~28–34). The record suggests a setting rich in volcanic glass with saline lake and/or pore waters (Owen et al., 2019), which is supported by diatom-inferred electrical conductivity data (Fig. 7) that also indicate variable lake depth. Palaeosols document episodic desiccation.

Biological calcite (ostracods, snail operculae) in GZ6 to GZ7 (~450–210 ka, Fig. 7) correlate with diatom-inferred shallow-water periods and higher salinities. *Limnocythere africana* strongly dominates and sometimes forms monospecific faunas. Such assemblages are today typical of alkalinity >30 meq L^{-1}. They are also abundant but co-

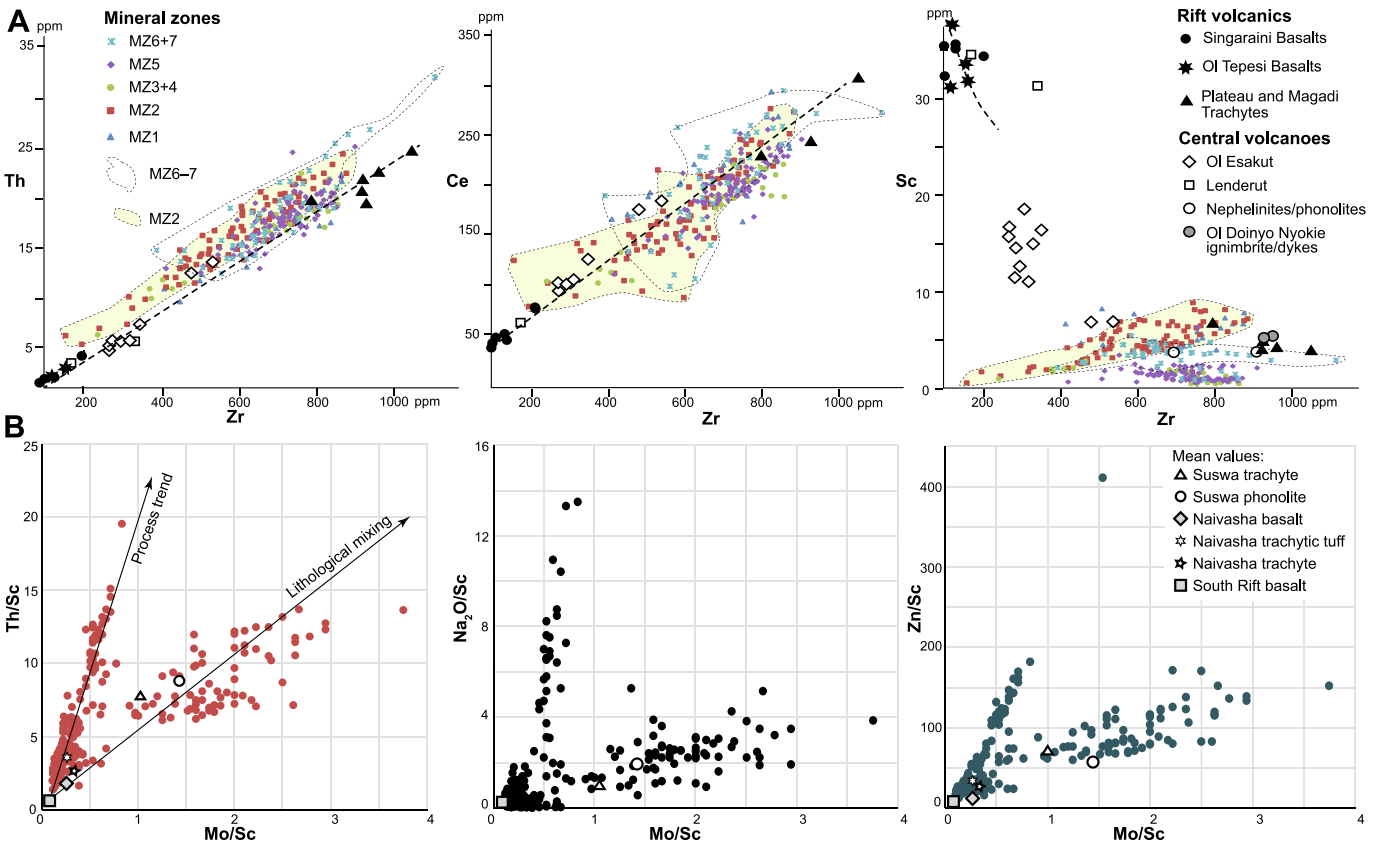

Fig. 6. Trace elements in core sediments and volcanics. Volcanic data from Le Roex et al. (2001). A: Trace elements (Th, Ce, Sc) plotted against Zr. Sample discrimination is best in plots of Sc. B: Trace elements (U, Na_2O, Zn) standardised against Sc. Note two distinctive trend lines reflecting: 1) mixing of different clastic sources and 2) process-related excursions.

occurring with other less saline/alkaline taxa at lower alkalinities, such as in Lake Turkana where alkalinity is 16–23 meq L^{-1} (Lindroth, 1953; Cohen et al., 1983; Cohen, 1986). Positive ostracod $\delta^{18}O$ values (1.04–3.00‰) suggest evaporative, closed-basin, saline lakes and correlate with diatoms that also indicate higher salinities (Fig. 7). In contrast, snail operculae show lower $\delta^{18}O$ values implying calcification in slightly fresher water, perhaps reflecting growth in a spring-fed lake margin or wetland, before being reworked into a more saline palaeolake. Alternatively, growth could have taken place during wetter periods at the same site indicating seasonal changes as in modern rift lakes (Olaka et al., 2016). The Mid-Pleistocene $\delta^{18}O$ values are more enriched than values from molluscs of Holocene Palaeolake Siriata in the southern Koora Graben, which, in contrast, reflect open, freshwater conditions (Dommain et al., 2022).

Strontium isotope ratios ($^{87}Sr/^{86}Sr$) in five fish bone samples from ostracod-bearing and non-ostracod-bearing sediments in GZ7 (Fig. 7) were all similar (0.7051 to 0.7055), indicating a stable water source, possibly from the eastern rift or from Lake Naivasha, which today produces water with similar $^{87}Sr/^{86}Sr$ ratios (Ojiambo et al., 2003; Olaka et al., 2022). Surface water from both areas would have flowed into the northern Koora Plain via a proto-Ol Keju Nyiro River, perhaps supplemented by groundwater from Lake Naivasha (Fig. 3A).

GZ8 is distinguished by a major reduction in Na_2O, indicating less extreme salinity, which is supported by an absence of zeolites. GZ8a is distinguished from GZ8b by increased CaO and Mg-calcite, indicating slightly greater salinity, although insufficient for zeolite formation. Diatoms indicate low lake levels with emergence documented by palaeosols. Arsenic is elevated, perhaps implying nearby hot springs. GZ8b is characterised by lower Na_2O and CaO suggesting fresher water, which is partially supported by diatom data, although the presence of saline-tolerant taxa (Muiruri et al., 2021c) implies episodic salinity increases. Some CaO may reflect pedogenesis. The palaeolake deepened into GZ8c times with a scarcity of diatom frustules reflecting reduced SiO_2.

GZ9 correlates with MZ7 and resembles much of GZ7c, showing considerable elemental variability. The distinctive peaks in Bi are repeated, with As concentrations similar to GZ7c. Na_2O varies, reaching high concentrations where analcime is present. Diatoms indicate fluctuating lake levels and salinities. Unconsolidated, younger, fluvial and wetland deposits above GZ9 accumulated after a permanent fall in lake level as the outlet to Lake Magadi (O3 in Fig. 3B) was cut, with the palaeolake retreating towards the southern Koora Graben (Muiruri et al., 2021c).

5.2. *Variability in selected trace elements, South Kenya Rift*

Regional interannual and longer time-scale climate change would have affected all South Kenyan basins simultaneously. In contrast, localised tectono-volcanic and/or geomorphic differences would potentially lead to contrasts in the spatial precipitation patterns, vegetation, river networks and sedimentation between each basin and the resulting mineralogical and geochemical records generated. The South Kenya Rift sediments document several phases when the geochemical records diverge with four major sets of geochemical change not correlating between the Koora, Olorgesailie and Magadi basins: 1) the Magadi Transition (MT), 2) the Magadi Tectonic Event (MTE), 3) the Koora Instability Period (KIP), and 4) the Trona Precipitation Period (TPP).

Sampling density decreases against time in the lower Koora and Magadi cores (Fig. 8), which will influence data variability. Nevertheless, the samples available from these intervals show little variation, except at Magadi during the MT (~770–700 ka) when the geochemical records begin to diverge, possibly reflecting hydrological separation as intervening horst blocks developed. Zr/TiO_2 and La/Lu ratios (Fig. 8)

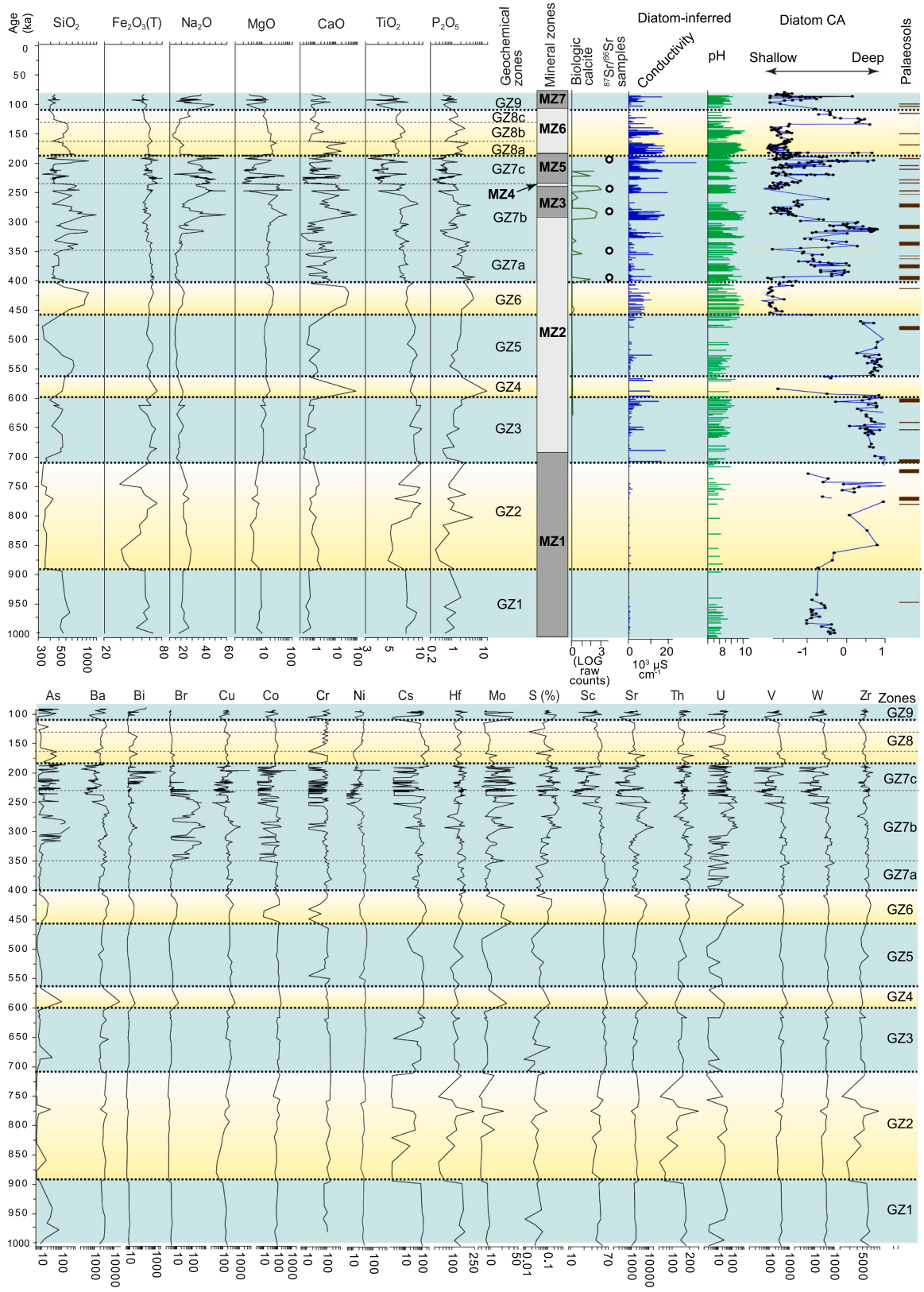

Fig. 7. Chronostratigraphy for selected elements and minerals. All data normalised ((x*100)/Al_2O_3). Geochemical zones GZ1–3 overlap with mineral zone MZ1. GZ3–8 are equivalent to MZ2–6 with GZ9 and MZ7 closely correlated. High silica values reflect both mineral and biological (mainly diatom) SiO_2. Elevated biological calcite data coincide with diatom-inferred shallow water phases. Data for $^{87}Sr/^{86}Sr$ samples are given in Table 3. Diatom Correspondence Analysis (CA) and palaeosol horizons from Muiruri et al. (2021c). Positive CA values correspond with deeper waters. Palaeosols indicate desiccation. Note many geochemical boundaries correlate with major changes in the diatom CA. Palaeosols are more common during periods of variability, as indicated by both geochemical and diatom data.

started to increase at Magadi, reflecting changing source lithologies as the western border fault formed (Deocampo et al., 2021). Owen et al. (2019) also reported increased Co, Cr, Cu and Ni, common in rift basalts, in MAG14-2A and suggested transport from the Kordija and Kirikiti Basalts along the base of the Nguruman Escarpment (Fig. 1). In contrast, during the MTE (~540 ka) there was a major reduction in these transition metals, which likely resulted from loss of cross-rift drainage as horsts evolved west of Magadi, causing stream diversion southwards to Lake Natron (Fig. 1A; Owen et al., 2019). However, the changes during both the MT and the MTE observed at Magadi are not reflected in the Koora sedimentary record, which shows relatively stable Zr/TiO_2 and La/Lu ratios (Fig. 8) from ~1000 to at least ~350–300 ka. Furthermore, Co, Cr, Cu and Ni (Fig. 7) are stable throughout this period at Koora, as are the same transition metals in Olorgesailie deposits (Owen et al., 2011). This major contrast probably reflects continuous supply of these elements by palaeorivers to both the Koora and Olorgesailie basins from basalts located on the eastern margins of the rift.

Deocampo et al. (2021) pointed out that increases in the redox-sensitive elements Mo, As and V in MAG14-2A (Magadi) represent euxinic conditions (anoxic, saline and sulfide-rich). These elements appear to have accumulated in very high concentrations only after the MT (Fig. 8) when the Magadi palaeolake became increasingly saline (Owen et al., 2019) and with euxinia cycles coinciding with high-orbital eccentricity. In contrast, the Koora record shows no major increases in these elements before ~325 ka. Further contrasts between Koora and Magadi after the MT are also evident in Na/Ca ratios (Fig. 8), reflecting contrasting lake salinities (Owen et al., 2018a).

The KIP (~325–180 ka) is characterised by increased element variability in OLO12-1A, but correlations between Koora and Magadi are poor (Fig. 8). Koora Zr/TiO_2 ratios increase modestly, suggesting a tephra contribution, with volcanic shards also increasing (Fig. 8) at a time when ash was accumulating at Olorgesailie (Deino et al., 2019). Koora sedimentation rates are highest between ~255 and 180 ka, again suggesting increasing fluvial volcanic inputs from the north (Deino et al., 2019) and/or increased erosion of ash across the palaeolandscape. Only a few thin Koora tephra are obviously air fall into quiet water. Increased inputs of volcanic ash/tephra at neighbouring Lake Magadi may have contributed to increased Zr/TiO_2 ratios there, but pervasive

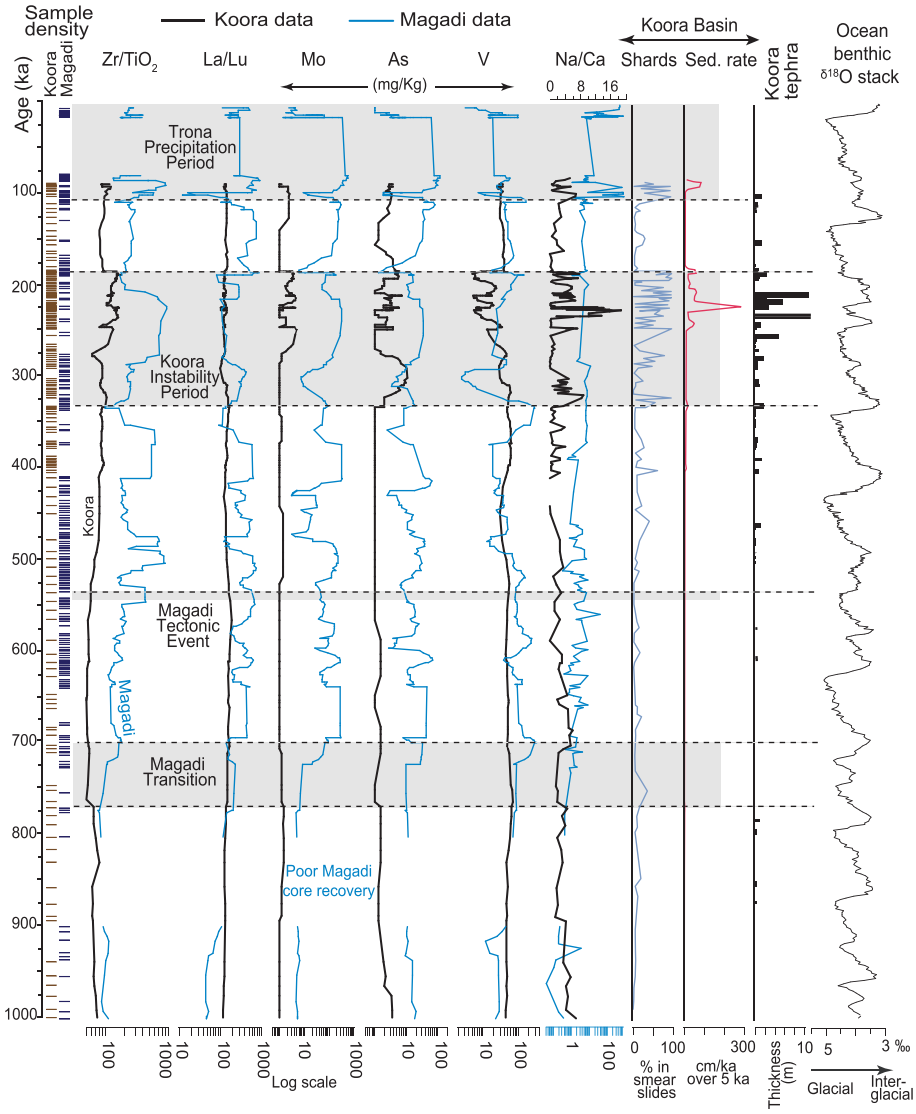

Fig. 8. Koora and Magadi core comparisons. Note the divergence of data from the Magadi Transition. The Magadi Tectonic Event records loss of transition metals and diversion of cross-rift drainage to Magadi (Owen et al., 2019). Transition metals are unchanged in the Koora Basin (Fig. 7). The Koora Instability Period represents increased variability in elemental data and coincides with increased tephra in the Olorgesailie Basin. The Trona Precipitation Period is recorded only at Magadi and likely records increased aridity combined with rising magmatic CO_2 along faults. Koora tephra events for OLO12-1 A, unit thickness in metres, after Deino et al. (2019).

zeolitisation, caused by highly saline alkaline waters, makes tephra identification difficult, except for one ash at ~328 ka (Owen et al., 2019).

Bromine (and S) concentrations increase significantly at Koora during much of the KIP interval, between ~340 and 225 ka, but with no equivalent increase at Magadi (Fig. 9). Deino et al. (2019) suggested that tephra was introduced to Koora and Olorgesailie by rivers from the Central Kenya Peralkaline Province (CKPP) to the north. Halogens, including Br, are strongly enriched in at least some peralkaline volcanics (Marks and Markl, 2017; Eggenkamp et al., 2021; Marshall et al., 2009). Although there is little available evidence for Br content in the CKPP, modern geothermal waters are enriched in bromide (Arusei, 1991). Furthermore, the volcanic centres of Longonot and Olkaria (Fig. 3A), located in the CKPP, were erupting from ~320 ka (Trauth and Strecker, 1996) close to the onset of increased Br at Koora. If this were the Br source, then three delivery mechanisms can be suggested: 1) fluvial, 2) atmospheric, or 3) groundwater.

The first could have delivered Br via the Ol Keju Nyiro-Kedong palaeodrainage (Fig. 1A). Only one Olorgesailie outcrop (B01/1B; Fig. 9) of KIP-age sediments from the Olkesiteti Member of the Oltulelei Formation (Behrensmeyer et al., 2018) was sampled and this contained little Br. This argues against fluvial transport or implies a different source for the B01/1B sediments. However, these limited analyses exclude thick KIP-age tuffs in other parts of the Olorgesailie Basin. If the Ol Keju Nyiro-Kedong palaeodrainage were the main Br source at Koora during the KIP interval, then its absence in Magadi sediments of the same age would argue against a direct fluvial link between the Magadi and Koora basins.

Secondly, BrO and SO_2 might have entered the atmosphere via eruption plumes (Gutmann et al., 2018), a process that is of increasing interest given the role BrO has in ozone depletion (Bobrowski et al., 2003; Boichu et al., 2011). If the Koora Br was derived from a gaseous

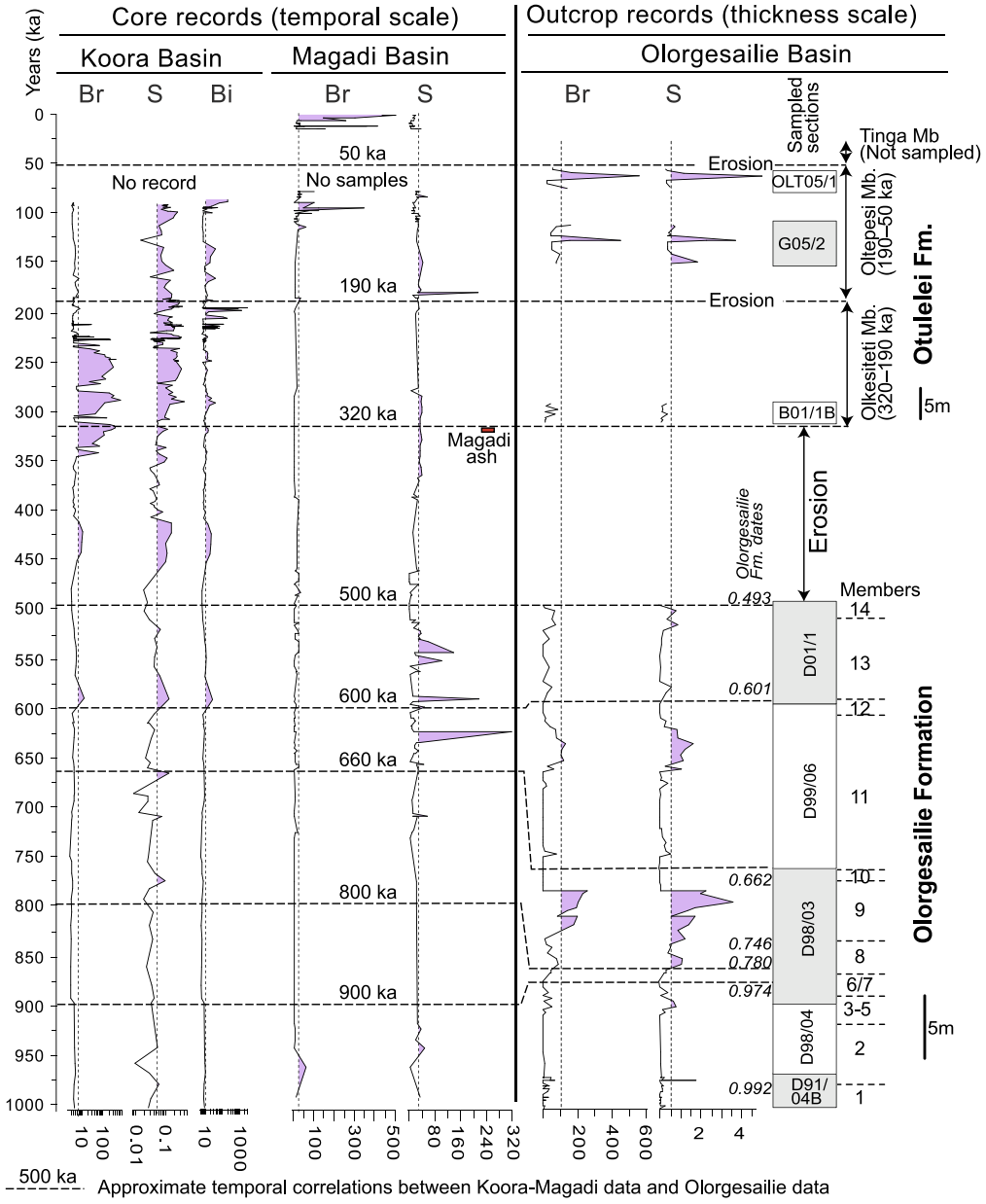

Fig. 9. Bromine, S and Bi records in the South Kenya Rift. Note minimal presence in most of these records with occasional spikes. Br at Koora is likely a volcanogenic indicator with high values at 340–225 ka, possibly reflecting activity to the north in the Central Kenya Peralkaline Province. Br at Magadi may reflect evaporative processes and does not correlate with Koora data. S may be partly volcanogenic but also reflects euxinia in lakes at Magadi. Bi may reflect localised spring activity. Olorgesailie dating is relatively weak, reflecting isolated dates in outcrops from different locations and is given only for broad comparison.

form or as aerosols, differences in concentrations between basins might reflect changing wind directions and/or variable volcanic sources. However, the small 10-km inter-basin distance would make this seem unlikely. Alternative sources are few but might have included Ol Doinyo Lengai, 95 km south of Magadi (Fig. 1A), which erupted recent natro-carbonatites with elevated Br concentrations of ~15 μg g^{-1} (Mangler et al., 2014) and 42–120 μg g^{-1} (Simonetti et al., 1997). This volcano has erupted periodically since about 0.5 Ma, but there are no relevant trace element records from the older volcanics to compare.

Thirdly, given modern southward subterranean flow (Allen et al., 1989; Becht et al., 2006), delivery might have involved Br-enriched groundwater from the CKPP. In contrast to the Koora Basin, the MAG14-2A Br data shows high Br in trona precipitated after ~105 ka during the TPP (Fig. 9). An alternative possibility for high Br concentrations might therefore involve evaporative concentration. Eugster, 1980 reported that Br acts conservatively during evaporation in Lake Magadi and reported dilute inflows of 0.04 mg kg^{-1} with evaporation leading to an increase to 22 mg kg^{-1} in groundwater, 180 mg kg^{-1} in intermediate brine and 310 mg kg^{-1} in saturated brine. He also noted that Br reaches 344 mg kg^{-1} in modern Magadi brines. Getenet et al. (2023) also reported enrichment in Br^{-} in Magadi and Nasikie Engida brines. However, this mechanism seems unlikely to account for the high Koora Br concentrations since it accumulated without trona and with diatoms, suggesting both fresher and saline episodes. Elevated Br may reflect different mechanisms at different times and places in the South Kenya Rift.

REE stratigraphies also point to subtle yet distinguishable processes in the three basins (Fig. 10). Koora core sediments are dominated by steep LREE and flat HREE patterns with a small negative Eu anomaly. This resembles Olorgesailie Formation sediment data and the dominant trachyte bedrock in the region. However, whereas some post-Olorgesailie Formation tufas also resemble trachyte patterns, others show HREE enrichment or Lu anomalies (Lee et al., 2013). Older Magadi samples display trachyte-type patterns, but with a major change after ~325 ka (early KIP times) when a variety of negative and positive anomalies develop. These changes probably reflect REE complexation with carbonate ions (Johannesson and Lyons, 1994) and were brought about by the development of hypersaline waters and perhaps increased Magadi spring/runoff ratios.

Potts et al. (2020) reported weak diatom, Si/K and phytolith orbital signals (11–17% of variance) from OLO12-1A with increased variability and palaeosol development after ~500 ka. Morlet wavelet analyses can reveal palaeoclimatic periodicities with the geochemical data presented here suggesting contrasts between the three basins that cannot be explained in climatic terms alone. Fig. 11 compares Morlet data for Zr/Ti and Mo from Koora and Magadi with ~21, 41 and 100 ka Milankovitch cycles indicated. The data show variable but generally non-significant power at these intervals with significant contrasts between Koora and Magadi. The Koora Zr/Ti ratios reflect clastic inputs and hint at a possible 41 ka cyclicity at ~700–550 ka after which power at 41 ka declines with a transition to higher power at 100 ka. In contrast, Magadi Zr/Ti ratios indicate higher power at 41 ka (and ~ 10 ka) at 820–620 and 320–210 ka. However, overall significant power spans a large range of frequencies and 41 ka power at the Equator is unlikely given that the influence of obliquity is relatively small there. In contrast, Mo reflects euxinia at Magadi (Deocampo et al., 2021) and displays a moderately strong 100 ka cyclicity and intermittent higher power at 41 and 21 ka before ~500 ka whereas the Koora data suggest higher power only after about 700 ka. The data variability might also partially reflect dating quality, which is weaker prior to ~500 ka for Koora and before 400 ka

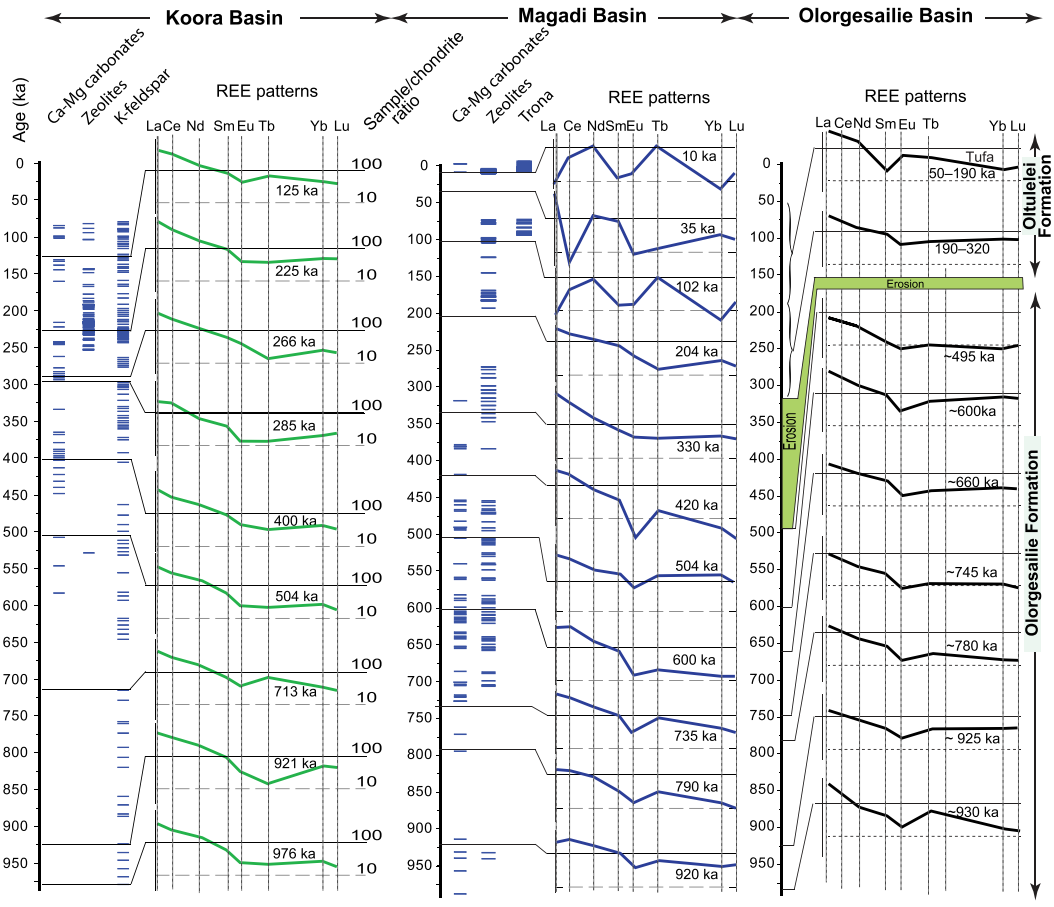

Fig. 10. Rare earth elements. Most patterns show steep LREE, an Eu anomaly and flat HREE, which reflects trachytic source rocks. These are similar throughout the Koora and Olorgesailie basins. Older Magadi sediments are similar but give way to many anomalies after about 325 ka when Magadi palaeolakes became hypersaline.

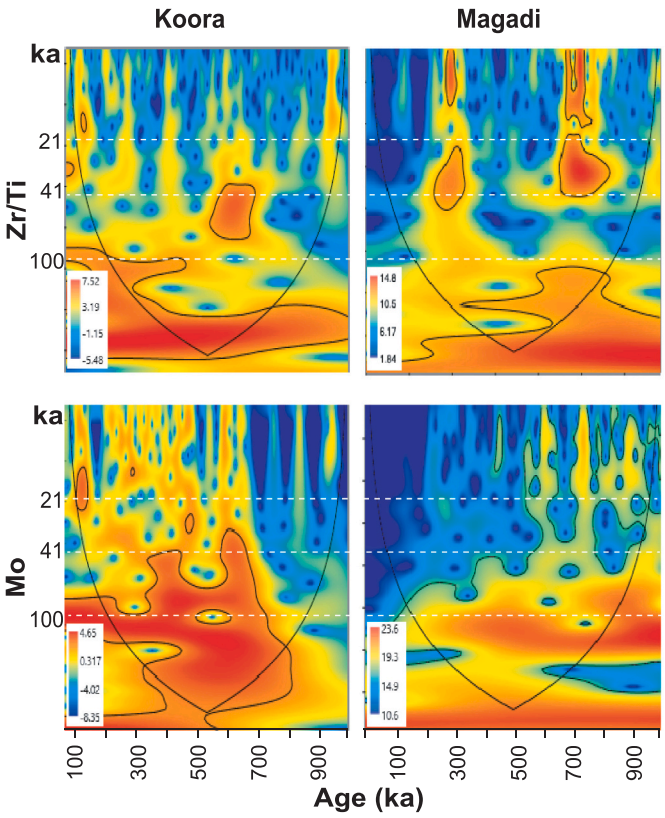

Fig. 11. Time series analyses for Zr/Ti and Mo from Koora and Magadi. Based on wavelets for unequal spacing in Past 4.14 software. Solid contour lines indicate significant (95% CI) wavelet amplitudes. Cone of influence delimits region not influenced by edge effects. Milankovitch cycles also plotted. See text for discussion.

for Magadi. Furthermore, mean sampling intervals varied between the basins (Koora = 3.3 ka; Magadi = 4.5 ka) and were at a lower resolution than previous diatom studies (Koora = 1.9 ka; Muiruri et al., 2021a, 2021c). The data comparisons in Fig. 11 imply possible climate controls but with differences that suggest that other factors are involved.

5.3. Regional comparisons

Muiruri et al. (2021a) compared Magadi and Olorgesailie diatom stratigraphies and recognised four environmental phases (Fig. 12). Freshwater lakes prevailed during Phase I (1000–750 ka) at Magadi with stable land surfaces at Olorgesailie. Koora diatoms and new geochemical data imply fresh to moderate salinities and low lake levels with palaeosols indicating occasional emergent intervals. Muiruri's Phase II (750–550 ka) was characterised by fresh to moderately saline lakes at Magadi and Olorgesailie, with Magadi pollen indicating wetter conditions across the region (Muiruri et al., 2021b). Differences between chronological models might explain some variation, but the Koora data suggest that the Phase I-II boundary should be placed somewhat earlier, at ~850 ka, during a period when Magadi pollen preservation and core recovery are relatively poor. Low diatom-inferred salinities and higher Ca/Na ratios at Koora indicate freshwater and consequently a palaeolake that periodically overflowed or had a subsurface outlet. At Magadi, Muiruri's Phase III (550–325 ka) was characterised by drier conditions than those of Phase II but with a wetter interval after ~400 ka (Muiruri et al., 2021a). Evidence at Olorgesailie is eroded. Outcrop distributions at Magadi suggest a tectonically induced lake retreat to the modern axial rift position after 375 ka (Owen et al., 2019). In contrast, the Koora data for an arid phase implies a more narrowly defined Phase III at 470–400 ka (Fig. 12).

Muiruri et al. (2021a) suggested Phase IV (~325–0 ka) at Magadi was characterised by continuous lacustrine conditions due to spring inflows but with an overall increase in aridity. Increasing ascending CO_2 along faults set against a drying climatic trend combined to trigger trona precipitation after 105 ka (Renaut and Owen, 2023). Muiruri et al. (2021a) also revealed that episodic floods entered the saline Magadi palaeolake during Phase IV. Koora geochemical variability and diatom data (Fig. 12) both suggest a slightly earlier onset for Phase 4 (~400 ka). However, placing of major transitions partly depends on which dataset is used. For example, while Koora tephra increase slightly after 400 ka, there is no substantial increase until about 270 ka (Fig. 8; Deino et al., 2019). Phytoliths suggest a transition to greater variability at 425–400 ka (Potts et al., 2020). Increased variability in leaf wax isotopes began at ~275 ka (Lupien et al., 2021). Different timings for change in these indicators may reflect contrasting spatial sourcing, e.g., phytolith variability (local and Koora Basin catchment), while leaf wax variability may represent the wider region.

Nevertheless, some climate signals are discernible in the Koora diatom conductivity, pH and lake depth records for this phase. Muiruri et al. (2021c) pointed out that, within chronological error ranges, several Phase IV Koora diatom-inferred deep-water stages correlate with neighbouring Magadi Basin floods and with global interglacials, but not all. Four examples of the latter correlations are shown in Fig. 12 by labelled arrows (5c, 5e, 7a and 9e) and tie lines. This partial correlation suggests that both climate (Lupien et al., 2021) and tectonic controls impacted the landscape and sedimentation. Multiple Koora palaeosols indicate repeated but short-term desiccation (Potts et al., 2020). In contrast, the Olorgesailie Basin was characterised by fluvial throughflow, springs, shallow ponds, land surfaces and incision during Phase IV (Behrensmeyer et al., 2018; Potts et al., 2018).

5.4. Controls on rift sedimentation

The sediments of the South Kenya Rift record climate impacts, but they also reflect the influence of tectonism, volcanism, and autocyclic sedimentary and geomorphological change. Our depositional model recognises that tectonism and volcanism may result in localised changes in different grabens. In addition, it is important to realise that similar palaeolandscapes may be generated through either climate change or tectonic/volcanic controls. Fig. 13, for example, shows two hypothetical pathways that could produce similar landscapes in 'throughflow' (Olorgesailie, Koora) and 'sump' (Magadi) basins caused by: 1) climate change only, or 2) tectonism and volcanism only. These would be difficult to distinguish in sedimentary records from single core sites (C1 and C2), but a careful examination of combined geochemical, microfossil and sedimentary clues can help to distinguish relevant controls, especially when records from adjacent basins are combined.

This study shows how varying climate, tectonism and volcanism have together changed the environments of the south Kenya Rift through the last million years. Climate change raised and lowered lake levels many times, with the Koora and Olorgesailie palaeolakes periodically drying out. In contrast, the Magadi Basin remained predominantly wet at the MAG14-2A site, reflecting its position in a regional sump with high spring inflow via faults, which also introduced silica from deep reservoirs and favoured chert formation (Owen et al., 2019; Renaut and Owen, 2023). The major depositional and geochemical contrasts reflect climate drivers but were also influenced by volcanism. Eruption of the 120-m-thick Magadi trachytes (~1.08 Ma below Magadi and Koora) infilled pre-existing basins, forming a relatively low-relief surface (Baker, 1958). Subsequent ash eruptions would have reduced accommodation space, especially during the latter part of the KIP (~325–180 ka) and stimulated zeolite formation due to increases in reactive volcanic glass.

Faulting and subsidence exerted a control on lake transgressions/regressions and help to explain miscorrelations between basin-scale palaeohydrology and global climate, particularly at Magadi.

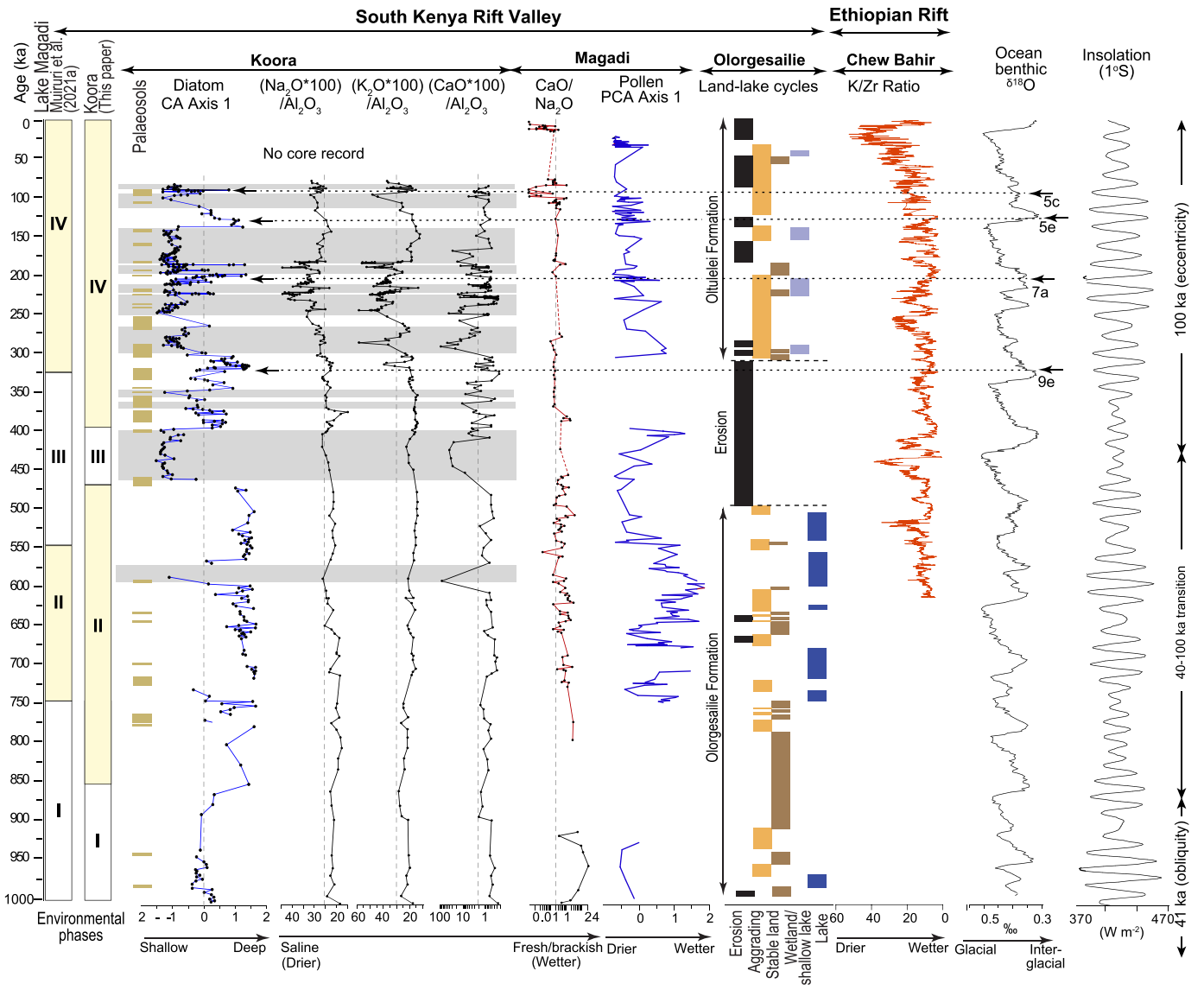

Fig. 12. South Kenya Rift and regional correlations. On left, four environmental phases based on Magadi data (Muiruri et al., 2021a) with time boundaries modified in this paper. Koora palaeosols indicate emergent periods superimposed on older lake sediments with diatom-based CA indicating shallow versus deep lakes. Grey bars represent low lake levels. Koora geochemical data arranged to show saline versus fresher lake conditions. Magadi (centre) Ca/Na_2O ratios reflect saline versus fresher conditions. Magadi pollen PCA indicates regionally wetter versus drier status (Muiruri et al., 2021b). Olorgesailie land-lake cycles modified after Potts et al. (2020). Regional Chew Bahir K/Zr, global $\delta^{18}O$ benthic foraminifera record and insolation at 1°S to the right for comparison (Cohen et al., 2022). Arrowed interglacials 5c, 5e, 7a, 9e correlate well with marked high lake levels in the diatom CA.

Accommodation space increased because of fracturing of the Magadi trachytes from at least ~1.2 Ma at Olorgesailie and ~ 1 Ma at Magadi and Koora, allowing lakes to form when the climate was favourable. While climate changes likely led to deeper lakes from about 850 ka, the changes during the MT probably reflect, at least in part, both regional subsidence of the rift axis and localised graben down-faulting. During the MTT (~540 ka), horsts diverted formerly west-east flowing streams southwards to Lake Natron. Continued faulting eventually resulted in the Magadi palaeolake retreating eastwards to its modern axial rift position by ~375 ka (Owen et al., 2019). Isaac (1978) and Behrensmeyer et al. (2002) attributed erosion at Olorgesailie after ~500 ka to fault-controlled base-level changes. During the last million years, there likely has been subsidence of ~50 m between the level of lacustrine tufa towers on horsts and the modern Lake Magadi surface, which overlies ~135–195 m of sedimentary infill (Owen et al., 2019). Muiruri et al. (2021c) also noted ~30 m of vertical movement prior to 80 kyr on a Koora Basin fault. Furthermore, regional southward tilting of the rift floor added to elevation variability. Eugster (1969), in a footnote, reported 10 m fault displacement of the High Magadi Beds (Late Pleistocene-early Holocene) along the western edge of Lake Magadi (Northwest Lagoon), and Hillaire-Marcel et al. (1986) similarly reported vertically displaced Late Quaternary high-level stromatolites southwest of Lake Magadi.

The development of trona at Magadi during the TPP (105–0 ka) suggests an increasingly dry climate that correlates well with regional data from Chew Bahir in Ethiopia (Fig. 12; Cohen et al., 2022), but this probably also reflects ascent of fault-controlled magmatic CO_2 (Owen et al., 2019). Late Quaternary faulting altered fluvial networks in ways that changed sedimentation. Fig. 3B shows the modern landscape and evidence for drainage alterations in the eastern South Kenya Rift (Crossley, 1976). Headward erosion by the Turoka River incised deeply into the eastern border fault escarpment as the rift subsided (Marsden, 1979), which delivered sediment to ephemeral Lake Kabongo where it partially infilled that basin. In contrast, the river shows minimal incision

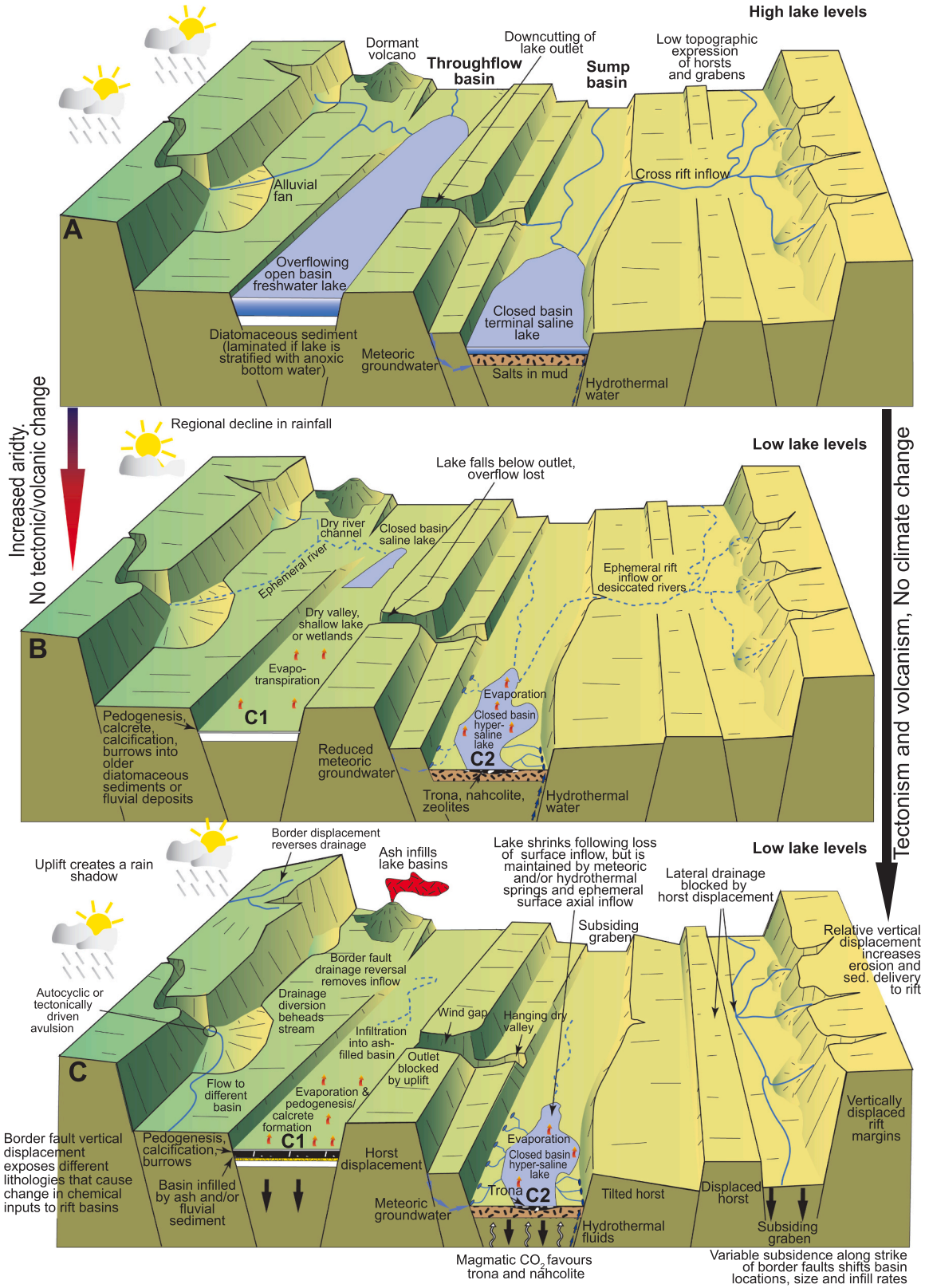

Fig. 13. Hypothetical models showing contrasting pathways that lead to similar landscapes. A: Initial landscape with overfilled lake entering a terminal lake also supplied by axial and cross-rift drainage. The Olorgesailie and Koora Basins are analogous to the marked 'Throughflow Basin' whereas the Magadi Basin is equivalent to a 'Sump Basin'. B: Simple aridification with no tectonism. Reduced rainfall causes lowered flow in rivers and consequent lake retreat and palaeosol or calcrete development in exposed areas. C: No climate change, but active tectonism, volcanism and autocyclic geomorphic processes. Avulsion causes drainage diversion (left rift margin) with reduced flow to lakes causing regression and palaeosols or calcrete to develop. Overflow to terminal lake lost. Vertical displacement of horst (right rift floor) diverts cross-rift drainage, reducing inflow. Springs along fault maintain shallower terminal lake. Cores at "C1" and "C2" would record similar settings. In reality, the environmental changes are driven by a combination of climate, volcanism, tectonism and geomorphic processes together.

into basalts (~2.3 Ma; Baker and Mitchell, 1976) forming the Singaraini Platform where the Turoka River is diverted by several horsts. In some cases, the river cut steep-sided wind (WG-2, Fig. 3B) and water gaps (WaG-1, WaG-3), indicating that it is antecedent to some of the faulting.

Faults control alluvial fans in the Kwenia Valley with implications for sedimentation. For example, a stream entering at D1 (Fig. 3B) formed a fan near a drainage divide where avulsion could then switch flow either north, leading to desiccation of Lake Kwenia, or south, favouring lake expansion. There are no core records, but avulsion switching would lead to alternating palaeosols and lake sediments at Kwenia even with no climate change. Further north, Marsden (1979) noted that the Loodo Ariak River previously flowed along an abandoned channel into Lake Kwenia. However, this may have been abandoned due to sediment accumulation at the D1 alluvial fan. Alternatively, headward erosion of the Ol Keju Nyiro River may have led to capture at D2, resulting in diversion away from Lake Kwenia and towards Olorgesailie, where some Oltulelei Formation fluvial-cross stratification indicates flow from the southeast.

Faulting also controls groundwater drainage, which can exert significant impact on the development of rift lakes, supplying water or providing drainage losses. For example, Lakes Naivasha and Baringo, in the central and northern Kenya Rift, are both freshwater bodies despite having no outlets. This is generally attributed to significant water loss through faulted volcanics in both areas (Allen et al., 1989; Dunkley et al., 1993; Clarke et al., 1990). Furthermore, Lake Magadi and the numerous springs in the area are today recharged mainly by groundwater from the Ewaso Ngiro, which lies to the west of Magadi and below the Nguruman Escarpment (Eugster, 1980). Renaut and Owen (2023) also note that aquifers are common in rift volcanics and that groundwater flow can be high. Permeability is created by cooling and tectonic joints, zones of lava autobrecciation, interconnected faults, contacts between lavas, especially along weathered surfaces or interbedded regosols, ash horizons and fluvial or lacustrine sediments.

The Siriata, Olkeri, Oloyeiti and Koora grabens were once occupied by a large palaeolake that extended over the Koora Plain. After ~83.5 ka, the palaeolake retreated from the Koora Plain (Potts et al., 2020) at least in part due to ~40 m of outlet downcutting (Muiruri et al., 2021c) at point O3 (Fig. 3B; Baker, 1986; Marsden, 1979). Collapse of a lava barrier at Lake Naivasha initiated a poorly-dated megaflood (Washbourn-Kamau, 1975, 1977; Baker and Mitchell, 1976; Crossley, 1976; Trauth et al., 2003) with dramatic sedimentological impacts on palaeodrainage. For example, Behrensmeyer et al. (2018) reported megaclast-bearing flood deposits in the Tinga Member (~50–36 ka) of the Oltulelei Formation (Olorgesailie) that may represent the same megaflood with finer deposits likely having reached the northern Koora Plain. Muiruri et al. (2021c) also reported a palaeoflood that overtopped a horst southwest of the Koora palaeolake with the escaping waters scouring parallel channels, depositing pebble bars and sediment on dry alluvial fans at the base of fault scarps (Fig. 3B).

6. Conclusions

Climate controls would have contributed to broadly synchronous changes in the three neighbouring South Kenya rift basins. However, contrasting sedimentary records developed because of differences in local environmental and sedimentological thresholds that, in turn, reflect tectonic, volcanic and geomorphological controls. Changes in the geochemical and microfossil records in the Koora Basin reflect global climate events, at least in part, with several higher lake levels and flood events correlating with interglacial stages. However, those records also include changes that are unrelated to climate. Correlations between Magadi and global climates can be made but are even less clear.

The Koora and Olorgesailie deposits preserve geochemical records that provide clues to past environmental change. Whereas several parameters (e.g., REE, transition metals) are similar, others are not (e.g., Br, Bi). In contrast, the Magadi Basin shows greater divergence in its geochemical records because of tectonic and volcanic controls, including those affecting spring input to the palaeolake. Four major periods are recognised that reflect the differences between Koora and Magadi: The Magadi Transition (MT), the Magadi Tectonic Event (MTE), the Koora Instability Period (KIP), and the Trona Precipitation Period (TPP).

These differences resulted from multiple factors. The Olorgesailie and Koora Basins reflect deposition: 1) along the same palaeoriver, which drained part of the axial rift and its eastern margins, at times linking to the Naivasha basin to the north; 2) in lakes that alternated between open and closed status as they rose to and fell below their outlets in throughflow basins; 3) in a setting where spring inflows were minor compared with fluvial inputs; and 4) that included volcaniclastic inputs derived from rivers and airfall. In contrast, Magadi has been characterised by: 1) inflow from rift axial rivers, but with only periodic connection to the Olorgesailie-Koora drainage system during wetter periods; 2) the presence of more continuous closed lakes even during drier episodes; 3) higher spring/river inflow ratios because of faulting and the basin location in a tectonic sump that favoured groundwater discharge from both meteoric and hydrothermal springs; 4) cross-rift drainage diversion related to horst formation during the MTE; 5) faults tapping magmatic CO_2 at depth, contributing to trona formation in a progressively drier climate during the TPP; and 6) the development of fault-controlled hot springs that introduced SiO_2 that formed chert.

Funding

Funding for this research was given for the Olorgesailie Drilling Project (ODP) by (1) the Peter Buck Fund for Human Origins Research, (2) the William H. Donner Foundation, (3) the Ruth and Vernon Taylor Foundation, (4) Whitney and Betty MacMillan, and (4) the Smithsonian Human Origins Program and (5) National Science Foundation grants EAR-1322017 and 1349599. Drilling at Magadi for the Hominin Sites and Paleolakes Drilling Project (HSPDP) was funded by ICDP and NSF grants (EAR-1123942, BCS-1241859, EAR-1338553). The Hong Kong Research Grants Council (HKBU201912) and several grants from NSERC Canada supported our work at both Koora and Magadi. CR thanks Univ. of Tübingen Excellence Strategy Grant: PRO-ROSCA-2021-11 for financial support.

CRediT authorship contribution statement

R. Bernhart Owen: Conceptualization, Data curation, Formal analysis, Funding acquisition, Investigation, Methodology, Project administration, Visualization, Writing – original draft, Writing – review & editing. **Nathan Rabideaux:** Formal analysis, Investigation, Methodology, Writing – review & editing. **Jordon Bright:** Formal analysis, Investigation, Methodology, Writing – review & editing. **Carolina Rosca:** Formal analysis, Investigation, Methodology, Visualization, Writing – review & editing. **Robin W. Renaut:** Formal analysis, Investigation, Writing – review & editing. **Richard Potts:** Conceptualization, Funding acquisition, Investigation, Project administration, Visualization, Writing – review & editing. **Anna K. Behrensmeyer:** Investigation, Visualization, Writing – review & editing, Conceptualization, Formal analysis. **Alan L. Deino:** Formal analysis, Investigation, Methodology, Visualization, Writing – review & editing, Conceptualization. **Andrew S. Cohen:** Conceptualization, Funding acquisition, Investigation, Project administration, Visualization, Writing – review & editing. **Veronica Muiruri:** Formal analysis, Investigation, Writing – review & editing. **René Dommain:** Formal analysis, Investigation, Writing – review & editing.

Declaration of Competing Interest

The authors declare that they have no known competing financial interests or personal relationships that could have appeared to influence the work reported in this paper.

Data availability

Data will be made available on request.

Acknowledgements

We thank the National Museums of Kenya for logistical and administrative support and the National Council for Science and Technology (NCSTI) for granting research permits. The Kenya Ministry of Petroleum and Mining and the National Environmental Management Authority of Kenya provided drilling and environmental permits. Local Maasai communities and Tata Chemicals Magadi provided field support. DOSECC Exploration Services supervised drilling that was undertaken by Drilling and Prospecting International (DPI). The LacCore and CSDCO facilities (University of Minnesota) allowed us to store and log our cores at their repository, and their staff have given important advice. This study is part of both the ODP publication series and HSPDP publication #55.

Appendix A. Supplementary data

Supplementary data to this article can be found online at https://doi.org/10.1016/j.palaeo.2023.111986.

References

Ahoulé, D.G., Lalanne, F., Mendret, J., Brosillon, S., Maïga, A.H., 2015. Arsenic in African waters: a review. Water Air Soil Pollut. 226, 302.
Allen, D.J., Darling, W.G., Burgess, W.G., 1989. Geothermics and hydrogeology of the southern part of the Kenya Rift Valley with emphasis on the Magadi-Nakuru area. Brit. Geol. Surv. Rep. SD/89/1.
Arusei, M.K., 1991. Hydrochemistry of Olkaria and Eburru Geothermal Fields, Kenya Rift Valley. UN University Geothermal Training Programme, Orkustofnun - National Energy Authority, Reykjavík, Iceland (Report No. 2).
Badertscher, S., Borsato, A., Frisia, S., Cheng, H., Edwards, R.L., Tüysüz, O., Fleitmann, D., 2014. Speleothems as sensitive recorders of volcanic eruptions – the Bronze Age Minoan eruption recorded in a stalagmite from Turkey. Earth Planet. Sci. Lett. 392, 58–66.
Baker, B., Mitchell, J.G., Williams, L.A.J., 1988. Stratigraphy, geochronology and volcano-tectonic evolution of the Kedong-Naivasha-Kinangop region, Gregory Rift Valley, Kenya. J. Geol. Soc. Lond. 145, 107–116.
Baker, B.H., 1958. Geology of the Magadi Area. Geol. Surv. Kenya Rep. 42.
Baker, B.H., 1986. Tectonics and volcanism of the southern Kenya Rift Valley and its influence on rift sedimentation. In: Frostick, L.E., Renaut, R.W., Reid, I., Tiercelin, J.-J. (Eds.), Sedimentation in the African Rifts, vol. 25. Geol. Soc. Lond. Spec. Publ, pp. 45–57.
Baker, B.H., 1987. Outline of the petrology of the Kenya rift alkaline province. In: Fitton, J.G., Upton, B.J.G. (Eds.), Alkaline Igneous Rocks, vol. 30. Geol. Soc. Lond. Spec. Publ, pp. 293–311.
Baker, B.H., Mitchell, J.G., 1976. Volcanic stratigraphy and geochronology of the Kedong-Olorgesailie area and the evolution of the South Kenya Rift Valley. J. Geol. Soc. Lond. 132, 467–484.
Baker, B.H., Goles, G.G., Leeman, W.P., Lindstrom, M.M., 1977. Geochemistry and petrogenesis of a basalt-benmoreite-trachyte suite from the southern part of the Gregory Rift, Kenya. Contrib. Mineral. Petrol. 64, 303–332.
Becht, R., Wango, M., Muno, F.A., 2006. Groundwater links between Kenyan Rift lakes. In: Odada, E.O., Olago, D.O., Ochola, W., Ntiba, M., Wandiga, S., Gichuki, N., Oyieke, H. (Eds.), Proc. 11th World Lakes Conf., Nairobi, Kenya, 2, pp. 7–14.
Behrensmeyer, A.K., Potts, R., Deino, A., Ditchfield, P., 2002. Olorgesailie, Kenya: A million years in the life of a rift basin. In: Renaut, R.W., Ashley, G. (Eds.), Sedimentation in Continental Rifts, vol. 73. SEPM Spec. Publ, pp. 97–106.
Behrensmeyer, A.K., Potts, R., Deino, A., 2018. The Oltulelei Formation of the southern Kenyan Rift Valley: a chronicle of rapid landscape transformation over the last 500 k.y. Geol. Soc. Am. Bull. 130, 1474–1492.
Bobrowski, N., Hönninger, G., Galle, B., Platt, U., 2003. Detection of bromine monoxide in a volcanic plume. Nature 423, 273–276.
Boichu, M., Oppenheimer, C., Roberts, T.J., Tsanev, V., Kyle, P.R., 2011. On bromine, nirogen oxides and ozone depletion in the tropospheric plume of Erebus volcano (Antarctica). Atmos. Enviorn. 45, 3856–3866.
Bright, J., 2017. Multi-Disciplinary Paleoenvironmental Context for the Integration of the Lower Colorado River Corridor, Bouse Formation, CA-AZ, USA, and Middle to Late Pleistocene Human Evolution, the Koora Plain, Southern Kenya. PhD thesis,. University of Arizona.
Brindley, G.W., Brown, G., 1980. Crystal Structures of Clay Minerals and their X-Ray Identification. Mineralogical Society, London.
Brooks, A.S., Yellen, J.E., Potts, R., Behrensmeyer, A.K., Deino, A.L., Leslie, D.E., Ambrose, S.H., Ferguson, J.R., d'Errico, F., Zipkin, A.M., Whittaker, S., Post, J., Veatch, E.G., Foecke, K., Clark, J.B., 2018. Long-distance stone transport and pigment use in the earliest Middle Stone Age. Science 360, 90–94.
Campisano, C.J., Cohen, A.S., Arrowsmith, J.R., Asrat, A., Behrensmeyer, A.K., Brown, E. T., Deino, A.L., Deocampo, D.M., Feibel, C.S., Kingston, J.D., Lamb, H.F., Lowenstein, T.K., Noren, A., Olago, D.O., Owen, R.B., Pelletier, J.D., Potts, R., Reed, K.E., Renaut, R.W., Russell, J.M., Russell, J.L., Schäbitz, F., Stone, J.R., Trauth, M.H., Wynn, J.G., 2017. The Hominin Sites and Paleolakes Drilling Project: Acquiring high-resolution paleoclimate records from the East African Rift System and their implications for understanding the environmental context of hominin evolution. PaleoAnthropology 1–43. https://doi.org/10.4207/PA.2017.ART104.
Chu, G., Sun, Q., Li, S., Lin, Y., Wang, X., Xie, M., Shang, W., Li, A., Yang, K., 2013. Minor element variations during the past 1300 years in the varved sediments of Lake Xiaolongwan, North-Eastern China. GFF 135, 265–272.
Clarke, M.C.G., Woodhall, D.G., Allen, D., Darling, G., 1990. Geological, Volcanological and Hydrogeological Controls on the Occurrence of Geothermal Activity in the Area Surrounding Lake Naivasha, Kenya. Report of the British Geological Survey and Ministry of Energy, Kenya.
Cohen, A., Arrowsmith, R., Behrensmeyer, A., Campisano, C., Feibel, C., Fisseha, S., Johnson, R., Dedaso, Z., Lockwood, C., Mbua, E., Olago, D., Potts, R., Reed, K., Renaut, R., Tiercelin, J., Umer, M., 2009. Understanding paleoclimate and human evolution through the Hominin Sites and Paleolakes Drilling Project. Sci. Drill. 8, 60–65.
Cohen, A., Campisano, C., Arrowsmith, R., Asrat, A., Behrensmeyer, A.K., Deino, A., Feibel, Hill A., Johnson, R., Kingston, J., Lamb, H., Lowenstein, T., Noren, A., Olago, D., Owen, R.B., Potts, R., Reed, K., Renaut, R., Schäbitz, F., Tiercelin, J.-J., Trauth, M.H., Wynn, J., Ivory, S., Brady, C., O'Grady, R., Rodysill, J., Githiri, J., Russell, J., Foerster, V., Dommain, R., Rucina, S., Deocampo, D., Billingsley, A., Beck, C., Dullo, L., Feary, D., Garello, D., Johnson, T., Junginger, A., Karanja, M., Kimburi, E., Mbuthia, A., McCartney, T., McNulty, E., Muiruri, V., Nambiro, E., Njagi, D., Norman, J., Rabideaux, N., Raub, T., Sier, M.J., Smith, P., Urban, J., Warren, M., Wondiymu, E., Yost, C., 2016. The Hominin Sites and Paleolakes Drilling Project: inferring the environmental context of human evolution from eastern African rift lake deposits. Sci. Drill. 21, 1–16.
Cohen, A.S., 1986. Distribution and faunal associations of benthic invertebrates at Lake Turkana, Kenya. Hydrobiologia 141, 179–197.
Cohen, A.S., Dussinger, R., Richardson, J., 1983. Lacustrine paleochemical interpretations based on eastern and southern African ostracodes. Palaeogeogr. Palaeoclimatol. Palaeoecol. 43, 129–151.
Cohen, A.S., Du, A., Rowan, J., Yost, C.L., Billingsley, A.L., Campisano, C., Brown, E., Deino, A.L., Feibel, C.S., Grant, K., Kingston, J.D., Lupien, R., Muiruri, V., Owen, R. B., Reed, K.E., Russell, J., Stockhecke, M., 2022. Plio-Pleistocene African environmental variability and mammalian evolution. Proc. Natl. Acad. Sci. 119 e2107393119.
Crossley, R., 1976. Structure, Stratigraphy and Volcanism in the Nguruman Escarpment Area of the Western Side of the Kenya Rift Valley. PhD thesis. University of Lancaster.
Crossley, R., 1979. The Cenozoic stratigraphy and structure of the western part of the Rift Valley in southern Kenya. J. Geol. Soc. Lond. 136, 393–405.
Crossley, R., Knight, R.M., 1981. Volcanism in the western part of the rift valley in southern Kenya. Bull. Volcanol. 44, 117–128.
Davies, G.R., Macdonald, R., 1987. Crustal influences in the petrogenesis of the Naivasha basalt–comendite complex: combined trace element and Sr-Nd-Pb isotope constraints. J. Petrol. 28, 1009–1031.
De Cort, G., Mees, F., Renaut, R.W., Sinnesael, M., Van der Meeren, T., Goderis, S., Keppens, E., Mbuthia, A., Verschuren, D., 2019. Late-Holocene sedimentation and sodium carbonate deposition in hypersaline, alkaline Nasikie Engida, southern Kenya Rift Valley. J. Paleolimnol. 132, 1–22.
Deino, A.L., Potts, R., 1990. Single crystal ^{40}Ar–^{39}Ar dating of the Olorgesailie Formation, southern Kenya Rift. J. Geophys. Res. 95 (B6), 8453–8470.
Deino, A.L., Behrensmeyer, A.K., Brooks, A.S., Yellen, J.E., Sharp, W.D., Potts, R., 2018. Chronology of the Acheulean to Middle Stone Age transition in eastern Africa. Science 360, 95–98.
Deino, A.L., Dommain, R., Keller, C.B., Potts, R., Behrensmeyer, A.K., Beverly, E.J., King, J., Heil, C.W., Stockhecke, M., Brown, E.T., Moerman, J., DeMenocal, P., The Olorgesailie Drilling Project Scientific Team, 2019. Chronostratigraphic model of a high-resolution drill core record of the past million years from the Koora Basin, South Kenya Rift: overcoming the difficulties of variable sedimentation rate and hiatuses. Quat. Sci. Rev. 215, 213–231.
Deocampo, D.M., Owen, R.B., Lowenstein, T.K., Renaut, R.W., Rabideaux, N.M., Billingsley, A., Cohen, A., Deino, A.L., Sier, M.J., Luo, S., Shen, C.-C., Gebregiorgis, D., Campisano, C., Mbuthia, A., 2021. Orbital control of Pleistocene euxinia in Lake Magadi, Kenya. Geology 50, 42–47.
Dericquebourg, P., Person, A., Ségalen, L., Pickford, M., Senut, B., Fagel, N., 2015. Environmental significance of Upper Miocene phosphorites at hominid sites in the Lukeino Formation (Tugen Hills, Kenya). Sediment. Geol. 327, 43–54.
Dommain, R., Riedl, S., Olaka, L.A., deMenocal, P., Deino, A., Owen, R.B., Muiruri, V., Müller, J., Potts, R., Strecker, M.R., 2022. Holocene bidirectional river system along

the Kenya Rift and its influence on East African faunal exchange and diversity gradients. Proc. Natl. Acad. Sci. 119 e2121388119.
Dunkley, P.N., Smith, M., Allen, D.J., Darling, W.G., 1993. The geothermal activity and geology of the northern sector of the Kenya Rift Valley. Brit. Geol. Surv. Res. Rep. SC/93/1.
Eggenkamp, H.G.M., Marks, M.A.W., Louvat, P., Markl, G., 2021. Bromine isotope variations in magmatic and hydrothermal sodalite and tugtupite and the estimation of Br isotope fractionation between melt and sodalite. Minerals 11 (4), 370.
Eugster, H.P., 1969. Inorganic bedded cherts from the Magadi area, Kenya. Contr. Mineral. Petrol. 22, 131.
Eugster, H.P., 1980. Lake Magadi, Kenya, and its precursors. In: Nissenbaum, A. (Ed.), Hypersaline Brines and Evaporitic Environments. Elsevier, Amsterdam, pp. 195–232.
Getenet, M., Otálora, F., Emmerling, F., Al-Sabbagh, D., García-Ruiz, J.M., 2023. Mineral precipitation and hydrochemical evolution through evaporitic processes in soda brines (East African Rift Valley). Chem. Geol. 616, 121222.
Guevara, S.R., Rizzo, A., Daga, R., Williams, N., Villa, S., 2019. Bromine as indicator of source of lacustrine sedimentary organic matter in paleolimnological studies. Quat. Res. 92, 257–271.
Gutmann, A., Bobrowski, N., Roberts, T.J., Rüdiger, J., Hoffmann, T., 2018. Advances in bromine speciation in volcanic plumes. Front. Earth Sci. 6, 213.
Halfman, J.D., Johnson, T.C., Showers, W.J., Lister, G.S., 1989. Authigenic low-Mg calcite in Lake Turkana, Kenya. J. Afr. Earth Sci. 8, 533–540.
Hardie, L.A., Eugster, H.P., 1970. The evolution of closed-basin brines. Mineral. Soc. Am. Spec. Pap. 3, 273–290.
Heinrichs, H., Schulz-Dobrick, B., Wedepohl, K.H., 1980. Terrestrial geochemistry of Cd, Bi, Tl, Pb, Zn and Rb. Geochim. Cosmochim. Acta 44, 1519–1533.
Herrick, R., 1972. Authigenic Minerals in the Pleistocene and Recent Sediments of Lake Magadi, Kenya. MSc thesis. University of Wyoming.
Hillaire-Marcel, C., Carro, O., Casanova, J., 1986. ^{14}C and Th/U dating of Pleistocene and Holocene stromatolites from East African paleolakes. Quat. Res. 25, 312–329.
Hudson, A.M., Quade, J., Ali, G., Boyle, D., Bassett, S., Huntington, K.W., De los Santos, M.G., Cohen, A.S., Lin, K., Wang, X., 2017. Stable C, O and clumped isotope systematics and ^{14}C geochronology of carbonates from the Quaternary Chewaucan closed-basin lake system, Great Basin, USA: Implications for paleoenvironmental reconstructions using carbonates. Geochim. Cosmochim. Acta 212, 274–302.
Isaac, G.L.L., 1978. The Olorgesailie Formation: Stratigraphy, tectonics and the palaeogeographic context of the Middle Pleistocene archaeological sites. In: Bishop, W.W. (Ed.), Geological Background to Fossil Man, vol. 6. Geol. Soc. Lond. Spec. Publ, pp. 173–206.
Johannesson, K.H., Lyons, W.B., 1994. The rare earth element geochemistry of Mono Lake water and the importance of carbonate complexing. Limnol. Oceanogr. 39, 1141–1154.
Le Roex, A.P., Späth, A., Zartman, R.E., 2001. Lithospheric thickness beneath the southern Kenya Rift: implications from basalt geochemistry. Contrib. Mineral. Petrol. 142, 89–106.
Lee, R.K.L., Owen, R.B., Renaut, R.W., Behrensmeyer, A.K., Potts, R., Sharp, W.D., 2013. Facies, geochemistry and diatoms of late Pleistocene Olorgesailie tufas, southern Kenya Rift. Palaeogeogr. Palaeoclimatol. Palaeoecol. 374, 197–217.
Lindroth, S., 1953. Taxonomic and zoogeographical studies of the ostracod fauna in the inland waters of East Africa: results of the Swedish East Africa Expedition 1948. Zool. Bietr. Uppsala 30, 43–156.
Lupien, R.L., Russell, J.M., Subramanian, A., Kinyanjui, R., Beverly, E.J., Uno, K.T., de Menocal, P., Dommain, R., Potts, R., 2021. Eastern African environmental variation and its role in the evolution and cultural change of *Homo* over the last 1 million years. J. Hum. Evol. 157, 103028.
Mangler, M.F., Marks, M.A.W., Zaitzev, A.N., Eby, G.N., Markl, G., 2014. Halogens (F, Cl and Br) at Oldoinyo Lengai volcano (Tanzania): Effects of magmatic differentiation, silicate–natrocarbonatite melt separation and surface alteration of natrocarbonatite. Chem. Geol. 365, 43–53.
Marchig, V., Gundlach, H., Möller, P., Schley, F., 1982. Some geochemical indicators for discrimination between diagenetic and hydrothermal metalliferous sediments. Mar. Geol. 50, 241–256.
Marks, M.A.W., Markl, G., 2017. A global review on agpaitic rocks. Earth Sci. Rev. 173, 229–258.
Marsden, M., 1979. Origin and Evolution of the Pleistocene Olorgesailie Lake Series. PhD thesis. McGill University, Montréal.
Marshall, A.S., Macdonald, R., Rogers, N.W., Fitton, J.G., Tindle, A.G., Nejbert, K., Hinton, R.W., 2009. Fractionation of peralkaline silicic magmas: the greater Olkaria Volcanic complex, Kenya Rift Valley. J. Petrol. 50, 323–359.
Masinde, A., Waswa, A., Muia, G., Makhanu, E., 2023. Spatial and temporal control of the volcanic activities over the distribution of sediments in the Magadi Basin, Kenya Rift. Sci. Afr. 22, e01935.
Maslin, M.A., Trauth, M.H., 2009. Plio-Pleistocene East African pulsed climate variability and its influence on early human evolution. In: Grine, F.E., Fleagle, J.G., Leakey, R.E. (Eds.), The First Humans: Origin and Early Evolution of the Genus *Homo*. Springer, Dordecht, pp. 151–158.
Maslin, M.A., Brierley, C.M., Milner, A.M., Schultz, Trauth, M.H, Wilson, K.E., 2014. East African climate pulses and early human evolution. Quat. Sci. Rev. 101, 1–17.
Moore, D.M., Reynolds, R.C., 1997. X-Ray Diffraction and the Identification and Analysis of Clay Minerals, 2nd edition. Oxford University Press, New York.
Muiruri, V.M., Owen, R.B., de Cort, G., Renaut, R.W., Rabideaux, N.M., Lowenstein, T.K., Leet, K., Sier, M., Cohen, A.S., Deocampo, D., Campisano, C.J., Billingsley, A., Mbuthia, A., 2021a. Middle Pleistocene to recent diatom floras and stratigraphy of the Magadi Basin, southern Kenya Rift. J. Paleolimnol. 65, 315–333.
Muiruri, V.M., Owen, R.B., Lowenstein, T.K., Renaut, R.W., Marchant, R., Rucina, S.M., Cohen, A., Deino, A.L., Sier, M.J., Luo, S., Leet, K., Campisano, C., Rabideaux, N.M., Deocampo, D., Shen, C.-C., Mbuthia, A., Davis, B.C., Alsossari, W., Wang, C., 2021b. A million year vegetation history and palaeoenvironmental record from the Lake Magadi Basin, Kenya Rift Valley. Palaeogeogr. Palaeoecol. Palaeoclimatol. 567, 110247.
Muiruri, V.M., Owen, R.B., Potts, R., Deino, A.L., Behrensmeyer, A.K., Reidl, S., Rabideaux, N., Beverly, E.J., Renaut, R.W., Moerman, J.W., Deocampo, D., Tyler Faith, J., Noren, A., Cohen, A.S., Shannon, K.B., Dommain, R., 2021c. Quaternary diatoms and palaeoenvironments of the Koora Plain, southern Kenya Rift. Quat. Sci. Rev. 267, 107106.
Neal, C., Neal, M., Hughes, S., Wickham, H., Hill, L., Harman, S., 2007. Bromine and bromide in rainfall, cloud, stream and groundwater in the Plynlimon area of mid-Wales. Hydrol. Earth Syst. Sci. 11, 301–312.
Ng'ang'a, P., Muchane, M.W., Johnson, T.C., Sturgeon, K., 1998. Comparison of isotopic records in abiogenic and biogenic calcite from Lake Turkana, Kenya. In: Lehman, J. T. (Ed.), Environmental Change and Response in East African Lakes. (Monographiae Biologicae 79). Springer, Dordrecht, pp. 173–190.
Ojiambo, S.B., Lyons, W.B., Welch, K.A., Poreda, R.J., Johannesson, K.H., 2003. Strontium isotopes and rare earth elements as tracers of groundwater–lake water interactions, Lake Naivasha, Kenya. Appl. Geochem. 18, 1789–1805.
Olaka, L.A., Wilke, F.D., Olago, D.O., Odada, E.O., Mulch, A., Musolff, A., 2016. Groundwater fluoride enrichment in an active rift setting: Central Kenya Rift case study. Sci. Total Environ. 545, 641–653.
Olaka, L.A., Kasemann, S.A., Sültenfuß, J., Wilke, F.D.H., Olago, D.O., Mulch, A., Musolff, A., 2022. Tectonic control of groundwater recharge and flow in faulted volcanic aquifers. Water Resour. Res. 58 e2022WR032016.
Owen, R.B., Potts, R., Behrensmeyer, A.K., Ditchfield, P., 2008. Diatomaceous sediments and environmental change in the Pleistocene Olorgesailie Formation, southern Kenya Rift Valley. Palaeogeogr. Palaeoclimatol. Palaeoecol. 269, 17–37.
Owen, R.B., Renaut, R.W., Potts, R., Behrensmeyer, A.K., 2011. Geochemical trends through time and lateral variability of diatom floras in the Pleistocene Olorgesailie Formation, southern Kenya Rift Valley. Quat. Res. 76, 167–179.
Owen, R.B., Renaut, R.W., Behrensmeyer, A.K., Potts, R., 2014. Quaternary geochemical stratigraphy of the Kedong–Olorgesailie section of the southern Kenya Rift valley. Palaeogeogr. Palaeoclimatol. Palaeoecol. 396, 194–212.
Owen, R.B., 2002. Sedimentological characteristics and origins of diatomaceous deposits in the East African Rift System. SEPM Spec. Publ. 73, 233–246.
Owen, R.B., Muiruri, V.M., Lowenstein, T.K., Renaut, R.W., Rabideaux, N., Luo, S., Deino, A.L., Sier, M.J., Dupont-Nivet, G., McNulty, E.P., Leet, K., Cohen, A.S., Campisano, C., Deocampo, D., Shen, C.-C., Billingsley, A., Mbuthia, A., 2018a. Progressive aridification in East Africa over the last half million years and implications for human evolution. Proc. Natl. Acad. Sci. 115, 11174–11179.
Owen, R.B., Renaut, R.W., Lowenstein, T.K., 2018b. Spatial and temporal geochemical variability in lacustrine sedimentation in the East African Rift System: evidence from the Kenya Rift and regional analyses. Sedimentology 65, 1697–1730.
Owen, R.B., Renaut, R.W., Muiruri, V.M., Rabideaux, N.M., Lowenstein, T.K., McNulty, E.P., Leet, K., Deocampo, D., Luo, S., Deino, A.L., Cohen, A., Sier, M.J., Campisano, C., Shen, C.-C., Billingsley, A., Mbuthia, A., Stockhecke, M., 2019. Quaternary history of the Lake Magadi Basin, southern Kenya Rift: tectonic and climatic controls. Palaeogeogr. Palaeoclimatol. Palaeoecol. 518, 97–118.
Potts, R., 1998. Variability selection in hominid evolution. Evol. Anthropol. 7, 81–96.
Potts, R., 2013. Hominin evolution in settings of strong environmental variability. Quat. Sci. Rev. 73, 1–13.
Potts, R., Faith, J.T., 2015. Alternating high and low climate variability: the context of natural selection and speciation in Plio-Pleistocene hominin evolution. J. Hum. Evol. 87, 5–20.
Potts, R., Behrensmeyer, A.K., Ditchfield, P., 1999. Paleolandscape variation and early Pleistocene hominid activities: members 1 and 7, Olorgesailie Formation, Kenya. J. Hum. Evol. 37, 747–788.
Potts, R., Behrensmeyer, A.K., Faith, J.T., Tryon, C.A., Brooks, A.S., Yellen, J.E., Deino, A. L., Kinyanjui, R., Clark, J.B., Haradon, C., Levin, N.E., Meijer, H.J.M., Veatch, E.G., Owen, R.B., Renaut, R.W., 2018. Environmental dynamics during the onset of the Middle Stone Age in eastern Africa. Science 360, 86–90.
Potts, R., Dommain, R., Moerman, J.W., Behrensmeyer, A.K., Deino, A.L., Riedl, S., Beverly, E.J., Brown, E.T., Deocampo, D., Kinyanjui, R., Lupien, R., Owen, R.B., Rabideaux, N., Russell, J.M., Stockhecke, M., deMenocal, P., Faith, J.T., Garcin, Y., Noren, A., Scott, J.J., Western, D., Bright, J., Clark, J.B., Cohen, A.S., Keller, C.B., King, J., Levin, N.E., Shannon, K.B., Muiruri, V., Renaut, R.W., Rucina, S.M., Uno, K., 2020. Increased ecological resource variability during a critical transition in hominin evolution. Sci. Adv. 6, eabc8975.
Rabideaux, N., 2018. Late Quaternary East African Environmental Change Based on Mineralogical and Geochemical Analysis of Outcrop and Core Material from the Southern Kenya Rift. PhD thesis. Georgia State University.
Rango, T., Vengosh, A., Dwyer, G., Bianchini, G., 2013. Mobilization of arsenic and other naturally occurring contaminants in groundwater of the Main Ethiopian Rift aquifers. Water Res. 47, 5801–5818.
Renaut, R.W., Owen, R.B., 2023. The Kenya Rift Lakes: Modern and Ancient. Springer, Berlin, Heidelberg.
Renaut, R.W., Owen, R.B., Lowenstein, T.K., de Cort, G., McNulty, E., Scott, J.J., Mbuthia, A., 2021. The role of hydrothermal fluids in sedimentation in saline alkaline lakes: evidence from Nasikie Engida, Kenya Rift Valley. Sedimentology 68, 108–134.
Roberts, N., Barker, P., 1993. Landscape stability and biogeomorphic response to past and future climatic shifts in intertropical Africa. In: Thomas, D.S.G., Allison, R.J. (Eds.), Landscape Sensitivity. Wiley, Chichester, pp. 65–82.

Ruttenberg, K.C., 2014. The global phosphorus cycle. In: Holland, H.D., Turekian, K.K. (Eds.), Treatise on Geochemistry, Volume 10 (Biogeochemistry). Elsevier, pp. 499–558.
Simonetti, A., Bell, K., Shrady, C., 1997. Trace- and rare-earth-element geochemistry of the June 1993 natrocarbonatite lavas, Oldoinyo Lengai (Tanzania): implications for the origin of carbonatite magmas. J. Volcanol. Geotherm. Res. 75, 89–106.
Stauffer, R.E., Jenne, E.A., Ball, J.W., 1980. Chemical studies of selected trace elements in hot-spring drainages of Yellowstone National Park. U.S.A. Geol. Surv. Prof. Paper, 1044-F.
Steffánsson, A., Anórsson, S., 2005. The geochemistry of As, Mo, Sb, and W in natural geothermal waters. Iceland. Proc. World Geotherm. Congr, Antalya, Turkey, p. 7.
Sun, S.-S., McDonough, W.F., 1989. Chemical and isotopic systematics of oceanic basalts: Implications for mantle composition and processes. In: Saunders, A.D., Norry, M.J. (Eds.), Magmatism in the Ocean Basins, vol. 42. Geol. Soc. Lond. Spec. Publ, pp. 313–345.
Surdam, R., Eugster, H., 1976. Mineral reactions in the sedimentary deposits of the Lake Magadi region, Kenya. Geol. Soc. Am. Bull. 87, 1739–1752.
Talbot, M.R., 1990. A review of the palaeohydrological interpretation of carbon and oxygen isotopic ratios in primary lacustrine carbonates. Chem. Geol. 80, 261–289.
Trauth, M.H., Strecker, M.R., 1996. Late Pleistocene lake-level fluctuations in the Naivasha Basin, Kenya. In: Johnson, T.C., Odada, E.O. (Eds.), The Limnology, Climatology and Paleoclimatology of the East African Lakes. Gordon and Breach, Amsterdam, pp. 549–557.
Trauth, M.H., Deino, A.L., Bergner, A.G.N., Strecker, M.R., 2003. East African climate change and orbital forcing during the last 175 kyr BP. Earth Planet. Sci. Lett. 206, 297–313.
Trauth, M.H., Bergner, A.G.N., Foerster, V., Junginger, A., Maslin, M.A., Schaebitz, F., 2015. Episodes of environmental stability and instability in late Cenozoic lake records of eastern Africa. J. Hum. Evol. 87, 21–31.
Varnavas, S.P., Cronan, D.S., 1988. Arsenic, antimony and bismuth in sediments and waters from the Santorini hydrothermal field, Greece. Chem. Geol. 67, 295–305.
Washbourn-Kamau, C.K., 1975. Late Quaternary shorelines of Lake Naivasha, Kenya. Azania 10, 77–92.
Washbourn-Kamau, C.K., 1977. The Ol Njorowa Gorge, Lake Naivasha basin, Kenya. In: Greer, D.C. (Ed.), Desertic Terminal Lakes. Utah Water Res. Lab, Logan, pp. 297–307.